active participation of the endocytic machinery. However, aS incorporation into cells is not completely disabled by the inhibition of endocytosis (3), indicating that other pathways, such as direct penetration, macropinocytosis, pore formation, and diffusion, might be involved in aS internalization (5). This notion is supported by previous studies showing that both monomers and oligomers of aS can freely passes though plasma membranes (4).

Because the aggregated aS in the brains of PD patients is robustly ubiquitinated (6–8), the ubiquitin modification of aS may regulate the biogenesis of LBs and could contribute to neurodegeneration in PD. Among the E3 ligases that catalyze aS ubiquitination, researchers have focused on Nedd4 (neural precursor cell expressed developmentally down-regulated protein 4) because this E3 ligase is highly expressed in neurons containing LBs and catalyzes the Lys-63-linked ubiquitination of aS (9, 10). Mammalian Nedd4 exists in two isoforms, Nedd4-1 and Nedd4-2. Structurally, the Nedd4 isoforms are composed of a C2 domain, 3–4 WW domains, which recognize proline-rich motifs (PP*X*Y or LP*X*Y) in substrate proteins (11, 12), and a catalytic domain homologous to the E6-AP C-terminal (HECT) domain at the C terminus. Nedd4-1 binds to the plasma membrane via the C2 domain in a Ca^{2+}-dependent manner (13) and controls the ubiquitination of membrane-bound receptor proteins, such as the epithelial Na^{+} channel (11). Modification by Lys-63-linked ubiquitination promotes the sorting of receptors for endocytosis and their subsequent degradation through the endolysosomal pathway (14). Given that Nedd4-1 exerts its E3 ligase activity in close proximity to the inner leaflet of the plasma membrane, the catalytic activity of Nedd4-1 likely acts preferentially on membrane-resident aS. In this study, we explored the possible mechanism by which the ubiquitination of aS by Nedd4-1 in the juxtamembrane cytoplasm could contribute to the incorporation and endosomal targeting of aS.

EXPERIMENTAL PROCEDURES

Cell Culture, Plasmid Preparation, and Transfection—SH-SY5Y human dopaminergic neuroblastoma cells (ATCC, Manassas, VA) were maintained in DMEM (Invitrogen) supplemented with 10% FBS (Thermo Scientific, MA) at 37 °C under humidified 5% CO_2/air. Triple FLAG-tagged human wild type Nedd4-1 was subcloned into the CMV10 vector. The HECT active-site dead mutant, C867A, and WW1–4-deleted (ΔWW) mutant were produced by PCR-based *in vitro* mutagenesis. The pEGFP-C1 plasmids encoding enhanced GFP-tagged human wild type-Rab5a, wild type-Rab7, and wild type-Rab11a were described previously (2). The DNA plasmids were isolated and purified using the GenoPure plasmid maxi kit (Roche Applied Science). 1×10^6 cells were transfected with 5 μg of plasmid DNA using the NEPA21 square wave electroporator (Nepa Gene, Chiba, Japan).

Recombinant Protein Purification—After the GST-wild type-aS(1–140) fusion construct was subcloned into the pGEX-6P-1 bacterial expression vector, the ΔPR1(1–119 and 129–140), ΔPR2(1–119 and 134–140), ΔC(1–119), P120A, P128A, and S129A aS constructs were produced using the PrimeSTAR® mutagenesis basal kit (TaKaRa, Otsu, Japan). All recombinant proteins were expressed in the BL21(DE3)pLysS *Escherichia coli* strain and purified as described previously (3). The purity and identity of the recombinant proteins were verified by Coomassie Brilliant Blue (MP Biomedicals, OH) staining and Western blot analysis. To verify the native state of recombinant aS, proteins were separated by blue native-PAGE (BN-PAGE). Briefly, the samples were charged by BN sample buffer (50 mM imidazole, pH 7.0, 50 mM NaCl, 5 mM 6-aminohexanoic acid, 0.5% Coomassie G-250, 1.0% digitonin, 20% glycerol) and then subjected to Any-KD™ TGX™ gradient gel (Invitrogen) with cathode buffer (0.02% Coomassie G-250, 50 mM Tricine, 7.5 mM imidazole, pH 7.0) and anode buffer (25 mM imidazole, pH 7.0). The proteins were electrophoresed for 20 min at 200 V, 4 °C, followed by a change of the Coomassie G-250 concentration of the cathode buffer to 0.002%, electrophoresis was continued for 60 min at 200 V, and then electroblotted onto a PVDF membrane.

In Vitro and in Vivo Ubiquitination Assays—The *in vitro* ubiquitination assay was performed according to the manufacturer's instructions (Enzo Life Sciences, New York). Briefly, 10 nM recombinant aS and 0.5 μg per reaction of the E3 ubiquitin ligase (E3) described below were incubated with 125 nM biotinylated ubiquitin, 5 nM E1 ubiquitin-activating enzyme (E1), 250 nM E2 ubiquitin-conjugating enzyme (E2), 250 μM Mg-ATP, and 10 units/ml inorganic pyrophosphatase (Sigma) at 37 °C for 30 min, and the reaction was quenched with 2× Laemmli buffer. All materials other than E3 and inorganic pyrophosphatase were obtained from Enzo Life Sciences. The E2s used were as follows: UbcH1, UbcH2, UbcH3, UbcH5a, UbcH5b, UbcH5c, UbcH6, UbcH7, UbcH8, UbcH10, and UbcH13/Mms2 (Enzo Life Sciences). The E3s used were as follows: SIAH-1 (Abnova, Taipei, Taiwan), SIAH-2 (Abnova), CHIP (Millipore), Hsp70 (Enzo Life Sciences), E6-AP (Boston-Biochem), Nedd4-1 (Abcam), and Nedd4-2 (Abnova).

RNAi Interference—To ablate Nedd4 expression in cultured cells, siRNA specifically targeting human Nedd4-1 (sc-41079, Santa Cruz Biotechnology) or Nedd4-2 (NEDD4LHSS118599, Invitrogen) or a scrambled control siRNA (sc-36869, Santa Cruz Biotechnology) was used. To silence human CHMP2B, a target-specific siRNA (sc-72895, Santa Cruz Biotechnology) was used. For human aS silencing, a 25-nucleotide-long siRNA was used, 5′-GACCAAAGAGCAAGUGACAAAUGUU-3′ (BONAC, Kurume, Japan) (15). SH-SY5Y cells in log phase growth were transfected with target-specific or control-scrambled siRNAs by electroporation. Then 24 h after gene silencing, 5 μM recombinant aS was added to the culture media, and the cells were incubated for another 24 h.

Subcellular Fractionation—For the subcellular fractionation of cultured cells, we adopted an established protocol (16). After being cultured for 24 h in medium containing 5 μM aS, the cells (1×10^7) were resuspended in 1 ml of ice-cold buffer (10 mM Tris/acetic acid, pH 7.0, and 250 mM sucrose) and homogenized using 20 strokes in a 2-ml Dounce tissue grinder. In some experiments, the cells were pretreated with 5 μM chloroquine (CQ, Sigma) and/or 10 μM MG132 (Millipore/Calbiochem) before exposure to aS. The cell homogenate was initially cleared by centrifugation (4000 × *g* for 2 min) to remove debris, undestroyed cells, plasma membrane, and nuclei. The supernatant was ultracentrifuged at 100,000 × *g* (Hitachi Koki Co., Ltd., Tokyo, Japan) for 2 min to pellet the mitochondria, endosomes,

and lysosomes (fraction EL). Lysosomes were isolated from fraction EL by osmotic lysis for 10 min using a 5:1 ratio (v/v) of pellet to water. After another centrifugation step at 100,000 × *g* for 2 min, the lysosomal proteins were recovered in the supernatant, and the mitochondria and endosomes remained in the pellet. The total protein in the culture media was extracted by trichloroacetic acid (TCA)/acetone precipitation and dissolved in 8 M urea, 5% SDS with sonication (2).

Western Blot Analysis—After measuring the protein concentration using a bicinchoninic acid protein assay kit (Thermo Scientific), lysates containing 20 μg of protein were electrophoresed, and the separated proteins were then electroblotted onto a PVDF membrane. After blocking with TBST containing 5% nonfat dry milk, the membranes were incubated with the following: anti-FLAG/M2 mouse monoclonal Ab (mAb) (1:1000, Sigma); anti-HA mouse mAb (1:1000, CST); anti-synuclein-1 mouse mAb (1:1000, BD Biosciences); anti-aS rabbit polyclonal Ab (pAb) (2628; 1:1000, CST); anti-aS mouse mAb (Syn211; 1:1000, Sigma); anti-SIAH-1 rabbit pAb (1:1000, Abnova); anti-SIAH-2 rabbit pAb (1:1000, Sigma); anti-CHIP rabbit pAb (1:1000, Santa Cruz Biotechnology); anti-Hsp70 (1:1000, StressGen); anti-E6AP mouse mAb (1:1000, Enzo Life Sciences); anti-Nedd4-1 rabbit pAb (1:1000, Abcam); anti-Nedd4-2 rabbit pAb (1:1000, CST); anti-BSA polyclonal Ab (1:2000, Santa Cruz Biotechnology); anti-Hsp90 mouse mAb (1:4000, StressGen); anti-ubiquitin Ab (P4D1; 1:1000, Santa Cruz Biotechnology); anti-Rab7 rabbit pAb (1:1000, CST); and anti-LAMP-2 mouse mAb (H4B4; 1:1000, DSHB). The primary antibodies were followed by HRP-conjugated secondary Ab (1:10,000, Jackson ImmunoResearch). The bands were visualized with the Luminata™ Forte Western HRP substrate (Millipore), and the images were captured using the Omega Lum G imaging system (Aplegen, Pleasanton, CA). All experiments were performed at least three times, and each of the bands was digitalized using ImageJ software (National Institutes of Health). Differences between the conditions were analyzed with Dunnett's multiple comparisons test using GraphPad Prism, version 6, for Mac OS X (GraphPad Software). The data are expressed as the means ± S.E.

Immunocytochemistry and Confocal Laser Scanning Microscopy—Recombinant aS was labeled with Alexa Fluor 488 or Alexa Fluor 555 reactive fluorescent dyes with tetrafluorophenyl ester binding (Invitrogen). Unattached dyes were carefully removed by size exclusion chromatography using Bio-Gel P-6 (Bio-Rad). Twenty four hours before the treatment with fluorophore-labeled aS (5 μM, 24 h), enhanced GFP-tagged Rab5a, Rab7, or Rab11a (markers for early, late, or recycling endosomes, respectively) was transfected into the SH-SY5Y cells. In some experiments, GFP-tagged human p62 expression constructs based on the baculovirus backbone (Premo Autophagy Sensors, Invitrogen) were co-transfected 16 h prior to the microscopic observation. To visualize lysosomes or mitochondria, the cells were treated with 100 nM LysoTracker® Green or 100 nM MitoTracker® Green for 30 min.

The cells were fixed in 4% (w/v) paraformaldehyde in phosphate-buffered saline (PBS) for 20 min, permeabilized with 0.5% Triton X-100 in PBS for 5 min, and blocked with 3% normal goat serum (Wako Pure Chemical Industries, Osaka, Japan) in PBS for 30 min. Anti-calnexin rabbit pAb (1:1000, StressGen), anti-PDI rabbit pAb (1:1000, StressGen), anti-syntaxin-6 rabbit mAb (1:100, CST), anti-ubiquitin mouse mAb (1:500, Millipore), anti-Nedd4-1 rabbit mAb (1:500, Abcam), and anti-CHMP2B rabbit pAb (1:500, Abcam) were used as primary antibodies and incubated for 18 h at 4 °C. Next, the cells were incubated with anti-mouse IgG Alexa Fluor 488 or 647 conjugates (1:2000, Invitrogen) for 1 h at room temperature. In some experiments, nuclei were counterstained by DRAQ7 (1:500, Biostatus, Leicestershire, UK). Fluorescent images were analyzed with the Olympus FV300 confocal laser scanning microscope system. All images were scanned by laser scanning microscope under identical conditions of 512 × 512 pixels with a 12-bit/pixel resolution. Under each set of conditions, 10–20 cells in six randomly chosen fields were analyzed to evaluate the sizes of the Rab7 vesicles that contain aS using ImageJ software (National Institutes of Health). The diameter of each vesicle was determined by comparison with a standard, and the differences between the conditions were analyzed with the Mann-Whitney *U* test using GraphPad Prism. The data are expressed as the means ± S.E.

Immunohistochemistry—Formalin-fixed, paraffin-embedded sections of the substantia nigra from five human patients with PD were subjected to immunohistochemical investigations using the avidin-biotin-peroxidase complex method with a Vectastain ABC kit (Vector Laboratories, Burlingame, CA). Polyclonal antibodies against Nedd4-1 (Sigma, 1:50; Millipore, 1:50) and Rab7A (Sigma, 1:50) were used as the primary antibodies. The sections were pretreated by heating for 15 min at 121 °C. Diaminobenzidine was used as the chromogen. The sections were counterstained with hematoxylin.

RESULTS

aS Is Internalized and Accumulates in the Endosomes of Neuronal Cells—First, we assessed the molecular weight of recombinant aS by BN-PAGE. The total recombinant aS migrated at ~40 kDa and showed two smaller peaks over 700 kDa (Fig. 1*a*). To eliminate the HMW aS species, recombinant aS was further separated using a 100-kDa pore-size filter, and LMW aS migrating at ~40 kDa was collected (designated as *<100-kDa aS* in Fig. 1*a*). To visualize the internalized aS, we prepared less than 100-kDa aS covalently bound to a fluorescent compound (Alexa-aS). The labeling efficiency was estimated to be ~2.29 (mol of dye)/(mol of protein) by fluorometric analysis (*Alexa-aS* in Fig. 1*b*). In BN-PAGE, Alexa-aS has two peaks, and the conformational changes might be caused during the process of fluorescence labeling or size exclusion chromatography (Fig. 1*c*). After treatment with 5 μM Alexa-aS for 24 h, acceptable amounts of internalized aS were detected in SH-SY5Y cells (Fig. 1*d*). Subcellular fractionation analysis revealed that internalized aS appeared in the cytosol in the early phase (8 h) and thereafter gradually increased to 24 h. However, the increased aS in the endosomes and lysosomes was inversely proportional to the cytosolic aS, indicating the translocation of cytosolic aS to endo/lysosomal compartments (Fig. 1*e*). The kinetics of aS re-secretion into the medium was similar to that of the cytosolic aS. It should be noted that the endosomal fraction isolated by our method contains both early and late endosomes because this fraction is positive for Rab5 and Rab7 (Fig. 1*e*). Next, we

performed immunocytochemical analysis using SH-SY5Y cells expressing enhanced GFP-tagged Rab5a, Rab7, and Rab11a together with the acidic organelle marker LysoTracker or the mitochondrial marker MitoTracker. Most of the internalized aS co-localized with Rab7-positive late endosomes and LysoTracker-positive structures and co-localized to a lesser degree with Rab5a-positive early endosomes and Rab11a-positive recycling endosomes. Note that none of the Alexa-aS corre-

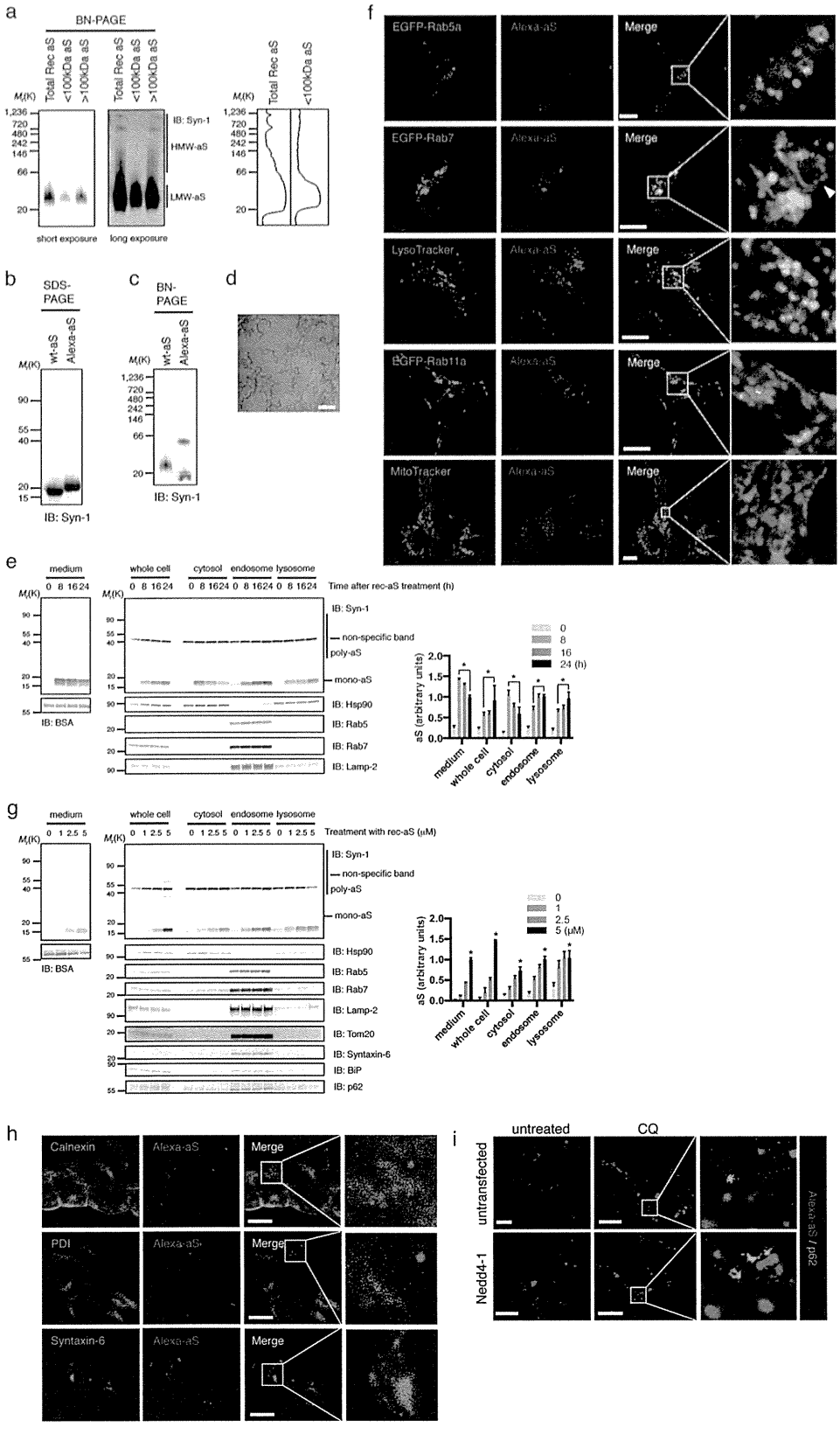

sponds with the fluorescence of MitoTracker (Fig. 1*f*). Another intriguing finding is that large Alexa-aS inclusions were occasionally surrounded by Rab7-positive vesicular structures. The level of internalized aS was in proportion to the amount of aS added to the culture medium (Fig. 1*g*). We also observed re-secreted aS in the medium 1 h after replacing it with fresh medium. The endosomal fraction used in this study also contains mitochondria, Golgi, autophagosomes, and endoplasmic reticulum because this fraction was positive for mitochondrial Tom20, the Golgi marker, syntaxin-6, the autophagosome marker p62, and the endoplasmic reticulum marker BiP (Fig. 1*g*). To exclude the possibility that internalized aS was located in these organelles, SH-SY5Y cells treated with Alexa-aS were fixed and subjected to double immunostaining. As shown in Fig. 1*h*, none of the Alexa-aS-positive red dots were co-localized with endoplasmic reticulum proteins (calnexin and PDI) or syntaxin-6. In addition, we performed p62 immunostaining using the aS-exposed, Nedd4-1-expressing cells in the presence of the autophagy inhibitor CQ (Fig. 1*i*). The treatment with CQ caused numerous p62-positive fluorescent puncta, indicative of autophagosomes; however, the Alexa-aS-positive puncta were scarcely co-localized with p62.

Nedd4-1 Catalyzes the Lys-63- and Lys-11-linked Polyubiquitination of aS—Several E3 ligases are known to catalyze the Lys-63-linked ubiquitination of aS, leading to its endolysosomal targeting and degradation (9, 17–20). To elucidate E3 ligase activity for aS, an *in vitro* aS ubiquitination assay was performed using the following human E3 ligases: SIAH-1, SIAH-2, Parkin, CHIP, Nedd4-1, and Nedd4-2 (Fig. 2*a*). In agreement with previous observations (9), we recapitulated that Nedd4-1 strongly catalyzed aS ubiquitination in the presence of UbcH5b. In addition, we found that the Nedd4-2 isoform equally ubiquitinates aS. The other E3 ligases failed to form ubiquitin chains on aS under the assay conditions employed. Nedd4-1 has been shown to prefer UbcH4, UbcH5b, UbcH5c, UbcH6, and UbcH7 as E2 ubiquitin-conjugating enzymes (21). To confirm this finding, aS ubiquitination by Nedd4-1 was re-evaluated with different E2 enzymes *in vitro*. We confirmed that UbcH5, UbcH6, UbcH7, and UbcH8 participated in the polyubiquitination by Nedd4-1 (Fig. 2*b*, *lower panel*). Among them, HMW aS-positive smears appeared solely in the samples containing UbcH5 and UbcH6 (Fig. 2*b*, *upper panel*). This finding is contradictory to a report by Tofaris *et al.* (9), which demonstrated that UbcH7 ubiquitinates aS together with Nedd4. This discrepancy could be due to different experimental conditions. Ubiquitin has seven lysine residues (Lys-6, Lys-11, Lys-27, Lys-29, Lys-33, Lys-48, and Lys-63), all of which can form ubiquitin chains, resulting in various structures that alter the target protein in different ways. To determine the types of ubiquitin linkages preferentially generated by Nedd4-1, recombinant wild type aS, together with Nedd4-1, was incubated with ubiquitin with no active lysine residues (Lys-0) or ubiquitin with only one active lysine residue (Lys-6, Lys-11, Lys-27, Lys-29, Lys-33, Lys-48, and Lys-63). A polyubiquitination smear exclusively appeared when the samples were incubated with wild type and Lys-63 ubiquitin (Fig. 2*c*, *lower panel*). Polyubiquitinated aS species were detected in the presence of wild type, Lys-11-, Lys-63, and to a lesser extent Lys-33 ubiquitin, showing that Nedd4-1 preferentially promotes the assembly of the Lys-63-linked ubiquitin chain (Fig. 2*c*, *upper panel*).

Lys-63 Linkage-specific Ubiquitination Enhances the Incorporation and Endosomal Targeting of Extracellular aS—After crossing the plasma membrane, some of the internalized aS exits the membrane, and some remains in the cytoplasm for minutes. To confirm this possibility, we performed pulse-chase experiments to determine how long internalized aS remains in the cytosolic fraction. After exposure to 5 μM recombinant aS for 24 h, the cells were extensively washed with PBS and further cultured for the indicated periods (0–60 min) in fresh medium in the absence of aS. The cytosolic fraction was isolated and subjected to Western blot analysis (Fig. 3*a*). After the removal of aS from the culture medium, the aS in the cytosolic fraction decreased by half within 5 min, demonstrating that the free cytosolic aS can easily cross the plasma membrane and immediately disappear from the cytosol. Based on these observations, it is tempting to speculate that specific ubiquitin modifications by Nedd4-1 might prevent aS secretion by leading to the juxtamembrane localization of aS to endosomal compartments. To confirm this possibility, we investigated whether Nedd4-1 silencing affects the re-secretion of internalized aS into the culture medium. As expected, after removing aS from the medium, Nedd4-1 silencing increased the aS re-secreted in the medium, whereas the elimination kinetics of cytosolic aS seem to be unaltered (Fig. 3, *a* and *b*). In addition to this re-secretion to the extracellular space, there are several possibilities that could explain the decrease of cytosolic aS as follows: proteolysis by the ubiquitin-proteasome system and

FIGURE 1. **Extracellular aS is readily internalized and accumulates in the endosomes of neuronal cells.** *a,* characterization of recombinant aS. On BN-polyacrylamide gels, a large peak around the molecular mass of 40 kDa, together with smears up to 200 kDa, are shown. Two small peaks over 700 kDa in recombinant aS were also detected (*HMW-aS* and *Total Rec aS*). After filtration with a 100-kDa pore size membrane, there is one peak at ~40 kDa (*LMW-aS* and *<100-kDa aS*). The results of densitometric analyses are shown in the *right panel*. *IB,* immunoblot. *b,* on SDS-polyacrylamide gels, denatured recombinant aS appears in its monomeric form at 18 kDa. After labeling with Alexa Fluor, a slight electrophoretic mobility shift was observed. *c,* Alexa-labeled aS forms two bands on a BN-polyacrylamide gel. *d,* internalized aS was observed in SH-SY5Y cells treated with 5 μM Alexa Fluor 488-aS for 24 h. *Scale bar,* 20 μm. *e,* after treating SH-SY5Y cells with 5 μM aS (below 100 kDa) for the indicated periods (0–24 h), internalized aS appeared in the cytosol in the early phase (8 h) and thereafter gradually decreased up to 24 h. Densitometry is shown in the *right panel*. The values for the amount of aS monomer in the medium, whole cell, cytosolic, endosomal, and lysosomal fractions were divided by the values of BSA, Hsp90, Hsp90, Rab7, or Lamp-2, respectively. *Asterisk*, $p < 0.01$ by Dunnett's multiple comparisons test. *f,* images show live cells after treatment with 5 μM Alexa Fluor 555-aS (*Alexa-aS*) for 24 h in the SH-SY5Y cells. Large (>2.5 μm) Alexa-aS-positive inclusions are surrounded by EGFP-Rab7-positive structures (*white arrowhead*). *Scale bar,* 10 μm. *g,* after treatment with recombinant aS, the level of internalized aS is in proportion to the amount of aS added to culture medium. One hour after changing with the fresh medium, re-secreted aS appears in the medium. Densitometry is shown in the *right panel*. *Asterisk*, $p < 0.01$ by Dunnett's multiple comparisons test against 0, 1, or 2.5 (μM). *h,* after treatment with 5 μM Alexa-aS for 24 h, SH-SY5Y cells were fixed and immunostained with organelle markers. The *inset* is a magnified picture of the square area. *Scale bar,* 10 μm. *i,* SH-SY5Y cells without or overexpressing Nedd4-1 were pretreated by 5 μM CQ for 2 h and further incubated in medium containing 5 μM Alexa-conjugated aS for 24 h. The *inset* is a magnified picture of the square area. *Scale bar,* 10 μm.

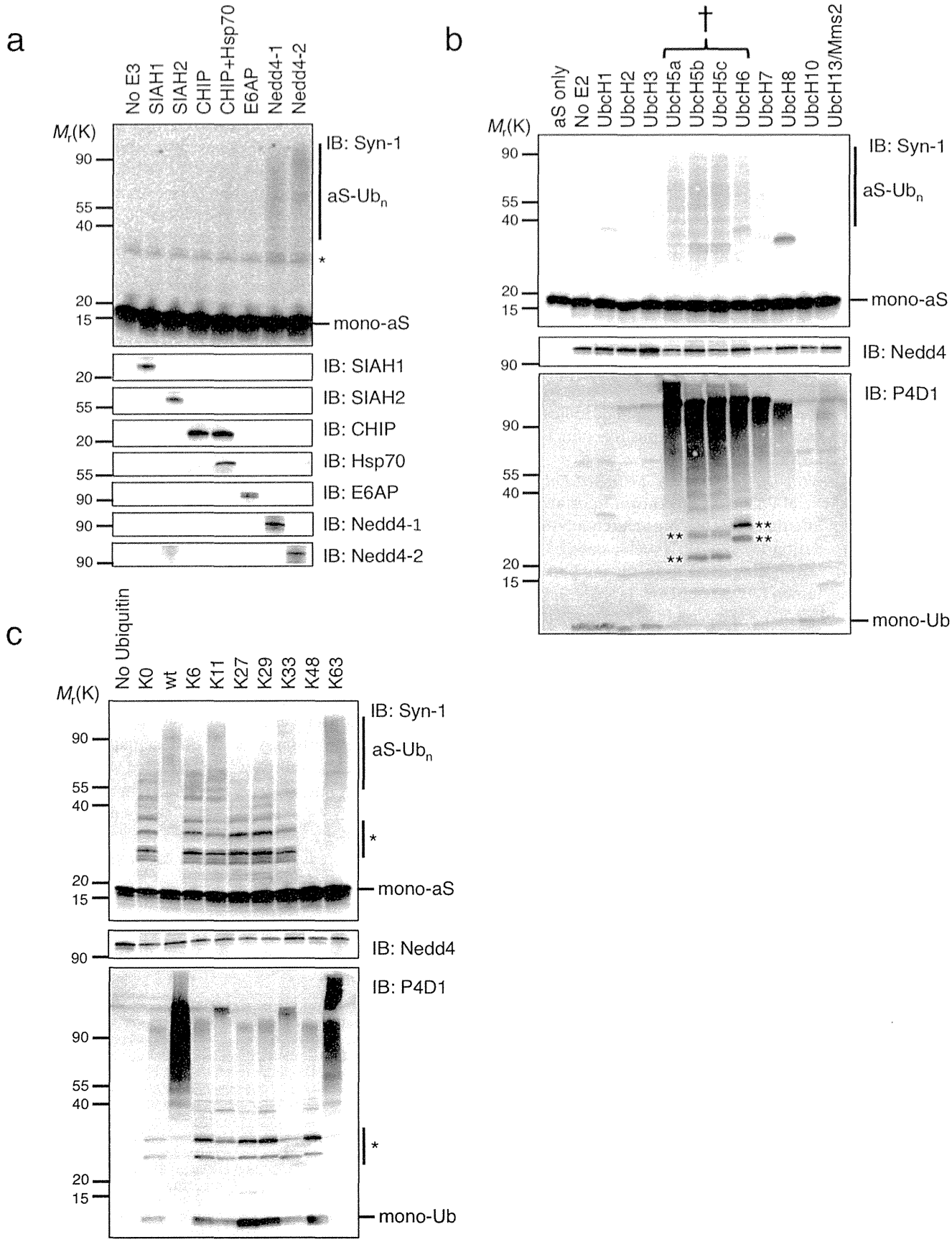

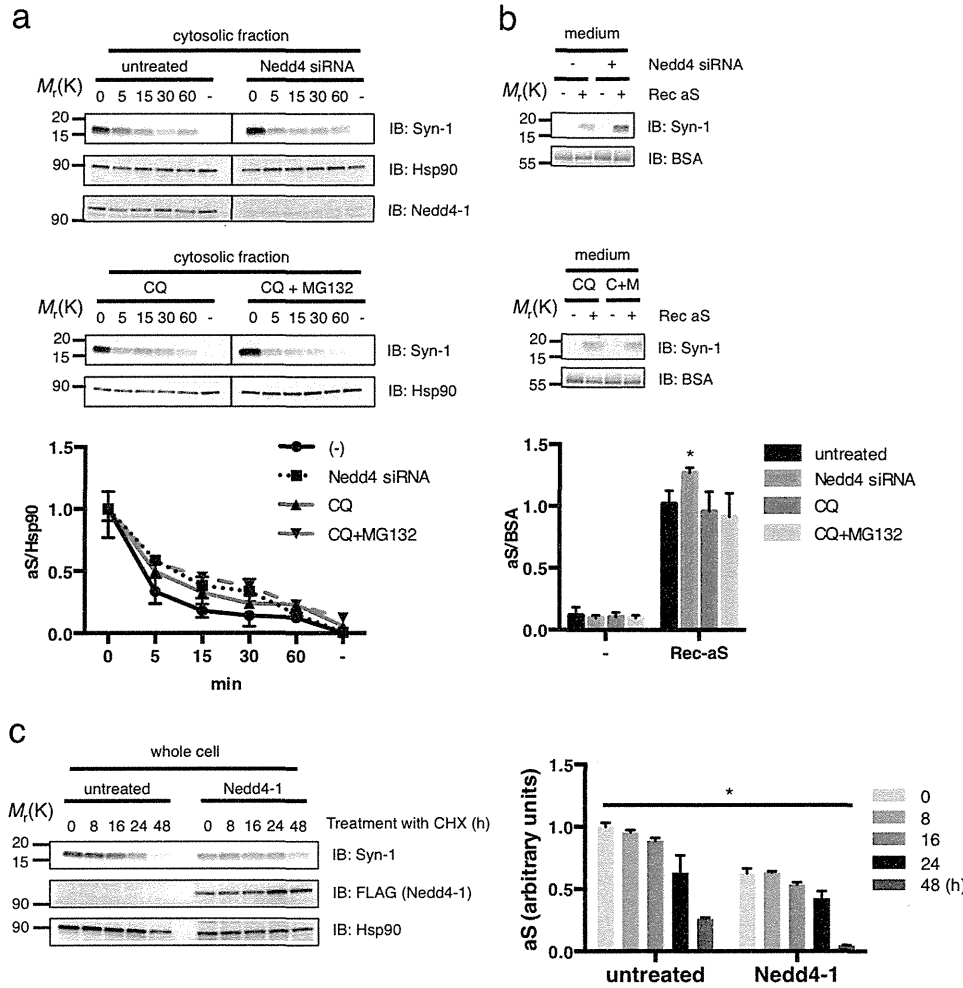

FIGURE 3. **Internalized aS is rapidly re-secreted to medium.** *a,* dynamic behavior of internalized aS was evaluated by pulse-chase experiments, using SH-SY5Y cells treated with 5 μM aS for 24 h. After the removal of aS from the medium, the amount of aS in the cytosol decreased by half within 15 min. A similar result was obtained in Nedd4-1-silenced cells (*upper panel*). Note that the autophagy/lysosome inhibitor CQ and/or proteasome inhibitor MG132 pretreatment did not alter the kinetics of aS elimination from the cytosol (*middle panel*). The results of densitometric analyses are presented in the *lower panel*. Statistical analyses were performed by Dunnett's multiple comparisons test. *IB*, immunoblot. *b,* to evaluate the aS re-secreted into the medium, the cells were incubated for 1 h with fresh medium after the aS exposure (5 μM for 24 h). Note that aS was detected in the medium treated with recombinant aS (*Rec aS*). Silencing of Nedd4-1 substantially increased the level of re-secreted aS (*upper panel*). CQ and/or MG132 (*CQ and C+M*) treatments did not affect the aS re-secretion. The results of densitometric analyses are shown in the *lower panel*. *Asterisk*, $p < 0.05$ by Dunnett's multiple comparisons test. *c,* Nedd4-1 expression affects the stability of endogenous aS. In the presence of the protein synthesis inhibitor cycloheximide (*CHX*), the basal amount of aS in cells overexpressing Nedd4-1 was significantly lower than that in the control cells (*asterisk*, $p < 0.01$ by Sidak's multiple comparisons test). Densitometry from three independent experiments is presented (*right panel*).

sequestration to autophagic degradation. To investigate this, we examined the rate of aS disappearance in the presence of CQ and proteasomal inhibitors (MG132). Of note, treatment with CQ and/or MG132 did not affect the aS turnover up to 60 min (Fig. 3, *a* and *b*). These results suggest that most of the aS that disappeared from the cytosol is not removed by lysosomal and/or proteasomal degradation. To investigate the effect of Nedd4-1 on the stability of extracellularly derived aS, we then investigated the time-dependent change of internalized aS in cells in the presence of the protein synthesis inhibitor cycloheximide. In the presence of 50 μg/ml cycloheximide, the basal amount of endogenous aS in Nedd4-1-expressing cells was significantly lower compared with control cells, but the decay kinetics of intracellular aS seem to be

FIGURE 2. **Nedd4-1 catalyzes the Lys-63-linked polyubiquitination of aS.** *a, in vitro* ubiquitination assay of aS with recombinant E3 ligases. Both human Nedd4-1 and Nedd4-2 equally catalyzed aS polyubiquitination (*aS-Ub$_n$*) in the presence of UbcH5b. Other E3 ligases failed to form ubiquitin chains on aS under the same conditions. *Asterisk* indicates the nonspecific bands. *IB*, immunoblot. *b,* aS ubiquitination by Nedd4-1 was evaluated with various E2 enzymes *in vitro*. Western blotting using P4D1 antibody, which recognizes both mono- and polyubiquitin, shows an HMW smear in the samples incubated with UbcH5a, UbcH5b, UbcH5c, UbcH6, UbcH7, and UbcH8 (*lower panel*). Mono-ubiquitin (*Ub*) bands are weakly apparent in each lane. E2 enzymes with one or two ubiquitins were occasionally detected (*double asterisk*). Note that the HMW aS smear (*aS-Ub$_n$*) visualized by anti-aS Ab (*Syn-1*) was solely detected in samples incubated with UbcH5a, UbcH5b, UbcH5c, and UbcH6. *c,* types of ubiquitin linkages preferentially generated by Nedd4-1. Recombinant wild type aS and Nedd4-1 were incubated together with ubiquitin that has no active lysine residue (Lys-0), or ubiquitin that has only one active lysine (*K*) residue (Lys-6, Lys-11, Lys-27, Lys-29, Lys-33, Lys-48, and Lys-63). Western blot using P4D1 antibody shows that the polyubiquitination smear is exclusively detected in the samples with wild type and Lys-63 (*lower panel*). Polyubiquitinated, HMW aS species were detected in the samples incubated with wild type, Lys-11, Lys-33, and Lys-63 ubiquitin (*upper panel*). Several bands at ~20–40 kDa are believed to be unspecific because these bands were also detected in the reaction with Lys-0 ubiquitin (*asterisk*).

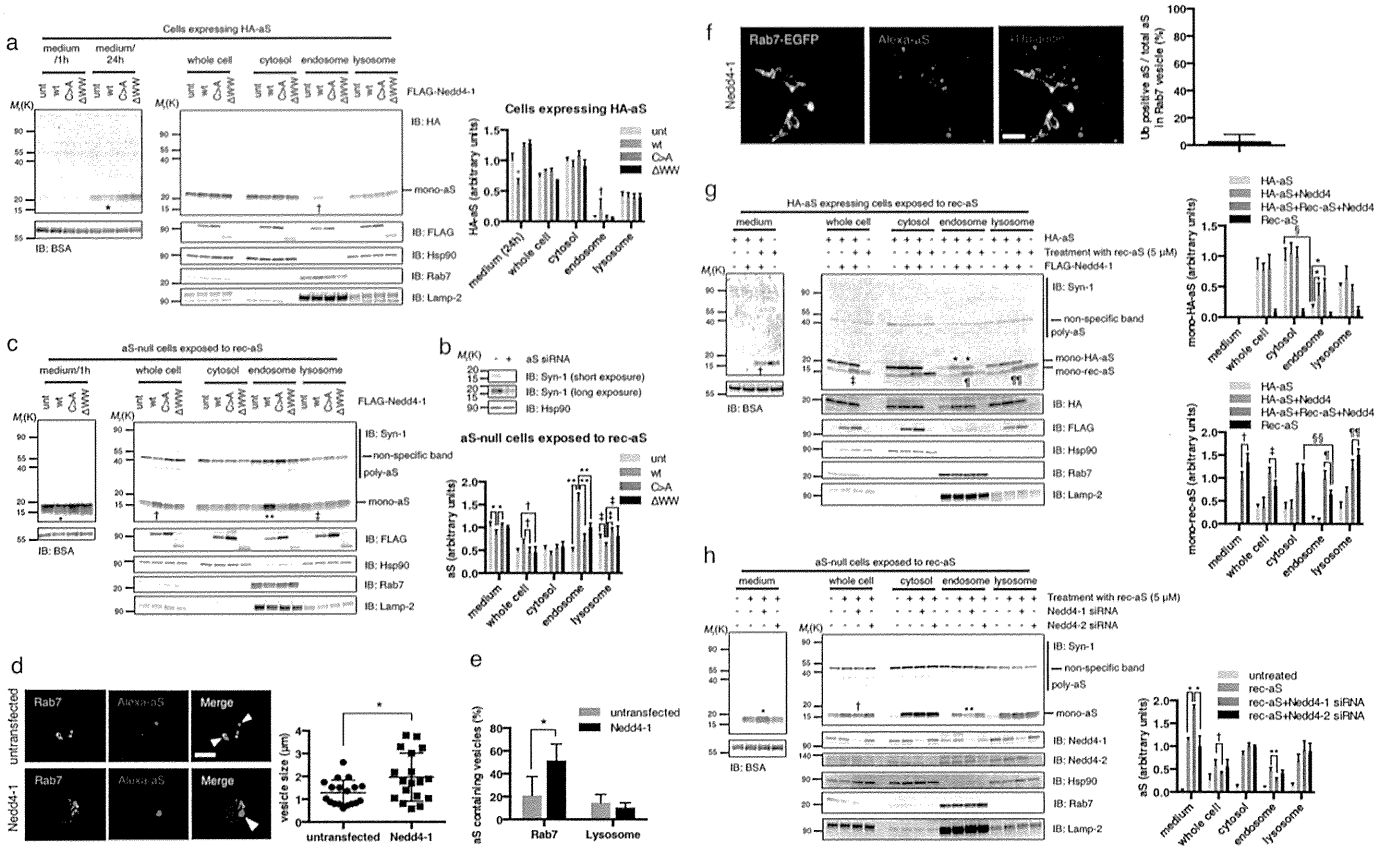

FIGURE 4. **Nedd4 facilitates the endosomal targeting of extracellularly derived and *de novo* synthesized aS.** *a,* Nedd4-1 facilitated the endosomal targeting of *de novo* synthesized aS in cultured cells. Wild type, C867A (*C>A*), or ΔWW Nedd4-1 was co-transfected into SH-SY5Y cells stably expressing HA-tagged wild type-aS. Following 48 h of Nedd4 expression, the amount of aS significantly increased in the endosomal fraction (*dagger*, $p < 0.05$) compared with the untransfected control (*unt*). Re-secreted aS levels decreased in the wild type Nedd4-1 overexpressing cells (*asterisk*, $p < 0.01$). The densitometric value of HA-aS in the medium, whole cell, cytosolic, endosomal, and lysosomal fractions were divided by the values of BSA, Hsp90, Hsp90, Rab7, and Lamp-2, respectively (*right panel*). *IB*, immunoblot. *b,* endogenous aS level substantially declined after 48 h of aS silencing in SH-SY5Y cells. *c,* Nedd4-1 targeted the extracellularly derived aS to the endosomal compartment. After silencing endogenous aS, SH-SY5Y cells were further transfected with Nedd4-1 constructs for 24 h, which was followed by aS exposure (5 μM for 24 h). Compared with the results in HA-aS-expressing cells (Fig. 4*a*), extracellularly derived aS tended to accumulate in the endosomal compartments. Furthermore, the ectopic expression of wild type Nedd4-1 considerably increased the amount of endosomal aS (*double asterisk*, $p < 0.01$). In contrast, the amount of aS in the medium and the lysosomal fraction slightly, but significantly, decreased in wild type Nedd4-1-expressing cells (*asterisk* and *double dagger*, respectively, $p < 0.05$). The densitometric values of monomeric aS in each fraction are presented in the *right panel*. *d,* Nedd4-1 expression significantly increased the size of aS-positive inclusions surrounded by Rab7-positive endosomal structures (*white arrows*) in SH-SY5Y cells exposed to Alexa-aS. *Scale bar,* 10 μm. *Asterisk*, $p < 0.05$ by two-tailed Mann-Whitney *U* test (*right panel*). *e,* number of Rab7-positive or Lysotracker-positive vesicles having Alexa-aS was quantitatively analyzed. *Asterisk*, $p < 0.01$ Sidak's multiple comparisons test. *f,* cells overexpressing Rab7-EGFP and Nedd4-1 were treated with Alexa-aS and then subjected to immunostaining. *Scale bar,* 10 μm. *g, de novo* synthesized HA-aS in the endosome was 20% *versus* the cytosolic aS (§). By contrast, the internalized recombinant aS was more extensively distributed in the endosome (50% compared with the cytosolic aS). (*dagger*, $p < 0.01$; *double dagger*, $p < 0.05$; *pilcrow*, $p < 0.05$; *double pilcrow*, $p < 0.05$; *asterisk*, $p < 0.05$ by Dunnett's multiple comparisons test). The densitometric values of mono-aS are shown in the *right panel*. In these cells, the level of endosomal aS was decreased (*double asterisk*, $p < 0.05$), whereas re-secreted aS was significantly increased (*asterisk*, $p < 0.001$). The densitometric values of monomeric aS in each fraction is presented in the *right panel*.

unchanged between control and Nedd4-1-expressing cells (Fig. 3*c*). We observed that Nedd4-1 did not influence the turnover of *de novo* synthesized HA-aS (data not shown).

Nedd4-1 Facilitates the Endosomal Targeting of aS—Intracellular aS is divided into two types based on its derivation as follows: aS internalized from the extracellular space and as *de novo* synthesized aS. Thus, the intracellular aS of different origins may have distinct fates during the process of intracellular vesicular transport. To determine whether Nedd4 specifies the intracellular trafficking of aS of different origins, we co-expressed wild type, C867A, or ΔWW Nedd4-1 in SH-SY5Y cells stably expressing HA-tagged aS. Following 48 h of Nedd4-1 expression, the amount of aS increased in the endosomal fraction (Fig. 4*a*). This finding is consistent with earlier research showing that Nedd4-1 promotes the endolysosomal sorting of aS for degradation (9). After washing off the medium, we did not detect re-secreted aS within 1 h, but a detectable amount of extracellular aS was observed up to 24 h (Fig. 4*a*). In an inverse correlation with endosomal aS, the level of re-secreted aS was slightly decreased in wild type Nedd4-1-overexpressing cells. To monitor the trafficking of extracellular aS in more detail, endogenous aS of SH-SY5Y cells was silenced prior to rec-aS exposure (Fig. 4, *b* and *c*). Compared with the results using HA-aS expressing cells, extracellularly derived aS tended to accumulate in the endosomal compartments (Fig. 4*c*). Furthermore, the ectopic expression of wild type Nedd4-1 substantially augmented the endosomal sorting of internalized aS. In contrast to the up-regulation of endosomal aS, we found that aS levels in the lysosomal fraction decreased slightly in Nedd4-1-expressing cells. The excessive amount of Nedd4-1 may have

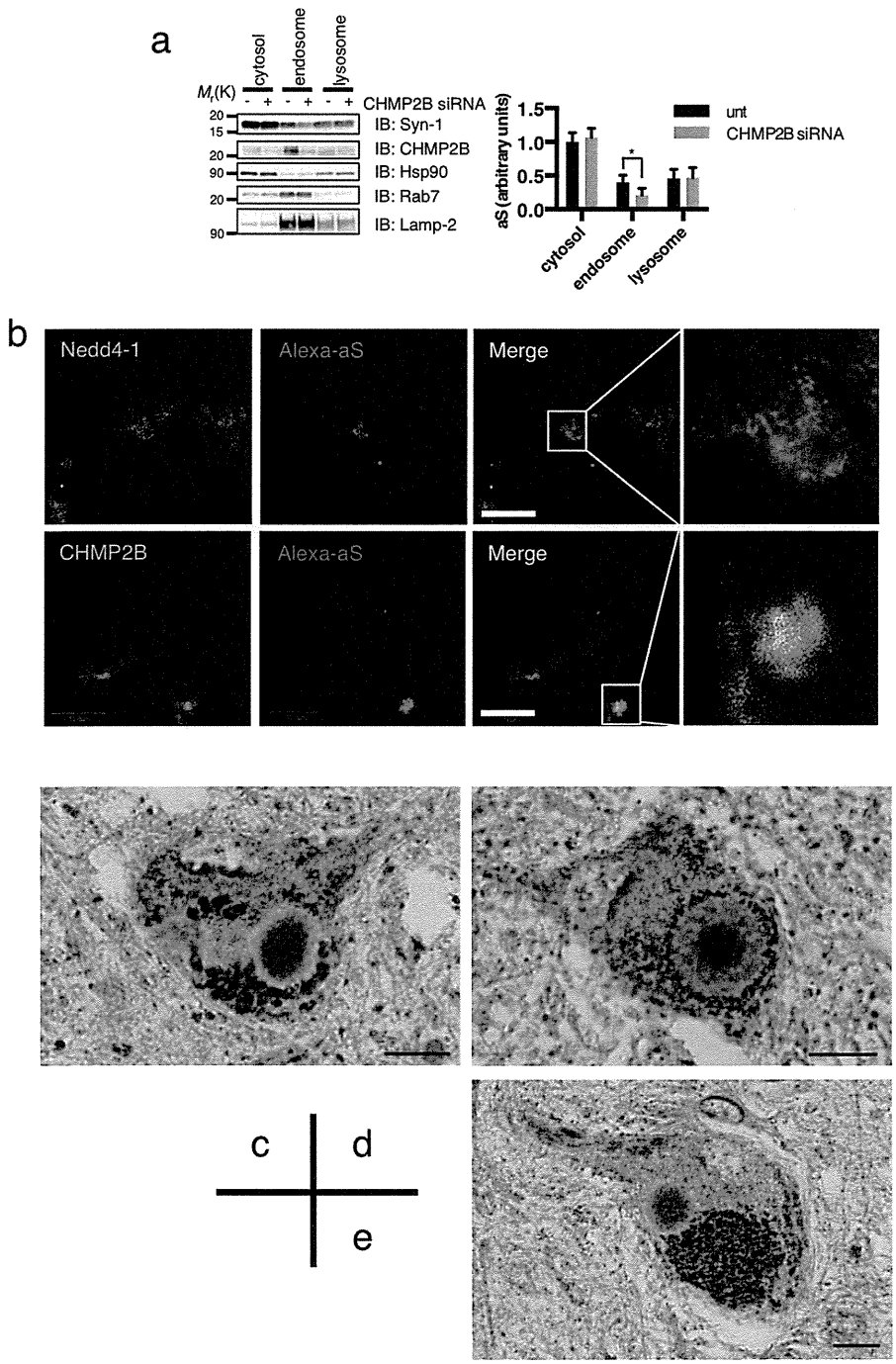

FIGURE 5. **Nedd4-1 accumulated to both *in vitro* and *in vivo* aggregate formations.** *a*, silencing of CHMP2B markedly reduced the amount of recombinant aS in the endosomes (*asterisk*, $p < 0.01$). The densitometric values of monomeric aS in each fraction are presented in the *right panel*. *IB*, immunoblot. *b*, immunocytochemical analyses of aS inclusions *in vitro*. Nedd4-1-expressing SH-SY5Y cells were treated with 5 μM Alexa-aS for 24 h and then subjected to immunostaining. aS-positive dense signal over 3 μm diameter was defined as an inclusion. Note that aS-positive inclusions were partly co-localized with Nedd4-1 and CHMP2B. *Scale bar*, 10 μm. *c–e*, immunohistochemical analysis of substantia nigra from postmortem PD brain. The core structure of Lewy bodies showed immunoreactivity with Rab7A (*c*), and Nedd4-1 (*d*, Millipore; *e*, Sigma). *Scale bar*, 10 μm.

hampered extracellularly derived aS transport from the endosome to the lysosome because Nedd4-1 expression significantly increased both the occurrence and size of aS-positive inclusions surrounded by Rab7-positive endosomal structures (Fig. 4, *d* and *e*). Theoretically, the cargo's ubiquitin modification needs to be detached before entry into the endosomal luminal space (22). Thus, it is feasible that only 3% of Alexa-labeled recombinant aS in Rab7-positive vesicles was ubiquitinated in this cellular model (Fig. 4*f*). The importance of ubiquitin-dependent sorting machinery is strengthened by the fact that the silencing of CHMP2B, a component of the endosomal sorting complex required for transport (ESCRT), resulted in a marked reduction of endosomal targeting of recombinant aS (Fig. 5*a*). As far as the subcellular distribution is concerned, *de novo* synthesized HA-aS in the endosome was 20% *versus* the cytosolic aS. By contrast, the internalized recombinant aS was more extensively

distributed in the endosome (50% compared with the cytosolic aS) (Fig. 4*g*). To further establish the role of Nedd4 in the endosomal targeting of aS, we knocked down endogenous Nedd4-1 or Nedd4-2 prior to aS exposure. As shown in Fig. 4*h*, a substantial decrease of endosomal aS and an elevation of extracellular aS were observed in Nedd4-1-deficient cells, although this effect was unremarkable in Nedd4-2-silenced cells. This finding may indicate that Nedd4-1 and Nedd4-2 are functionally distinct and that Nedd4-1 is the main human Nedd4 isoform that affects the fate of internalized aS in human neuronal cells.

Nedd4-1 Is a Component of aS-positive Inclusions in Cellular Model and the Brain Lesion of PD—To verify the functional role of Nedd4-1 in the formation of aS-positive inclusions, SH-SY5Y cells transfected with Nedd4-1 were treated with Alexa-aS for

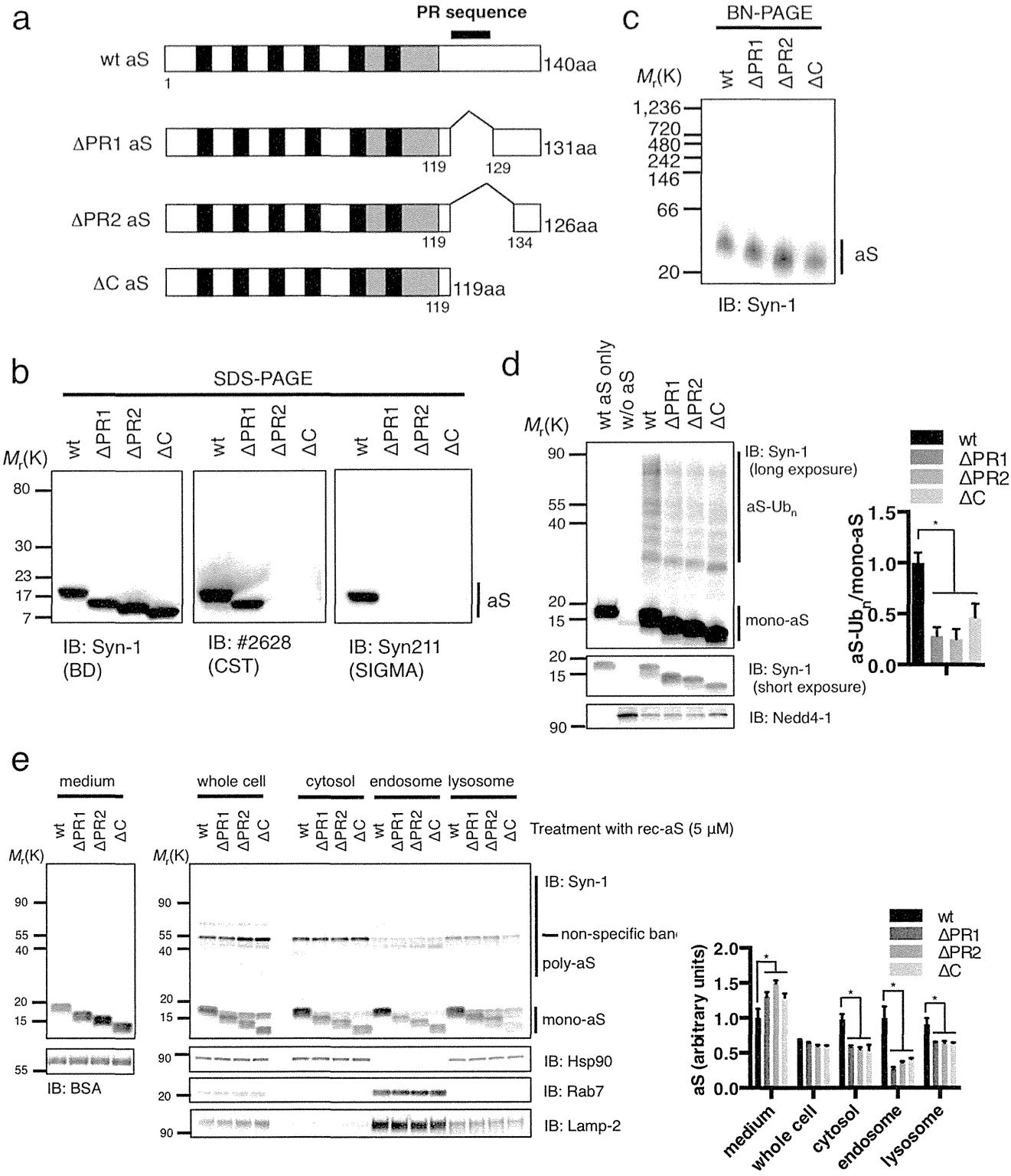

24 h and then subjected to double immunostaining. As shown in Fig. 5*b*, aS-positive inclusions were partly positive for Nedd4-1 and a component of ESCRT machinery, CHMP2B. This outcome indicates that the ESCRT pathway is closely involved in the process of aS inclusion formation. Furthermore, we found that the core structure of LBs, a pathological hallmark of PD, showed strong immunoreactivity with Rab7A (Fig. 5*c*) and Nedd4-1 (Fig. 5, *d* and *e*).

C-terminal Residues of aS Are Required for Nedd4-1-mediated Endosomal Targeting—Nedd4-1 recognizes PR regions of target proteins via the WW domain, thereby exerting its E3 ligase activity. Although aS does not have a canonical PP*X*Y motif, it contains a relatively proline-rich domain (PVDPDNEAYEMPSEEGYQDYEPEA) at its C terminus (9). To determine the functional importance of the PR sequence in Nedd4-1-mediated ubiquitination, three deletion mutants of aS, designated ΔPR1(1–119 and 129–140), ΔPR2(1–119 and 134–140), and ΔC(1–119), were generated and expressed in *E. coli* (Fig. 6, *a* and *b*). To discriminate among these mutants by Western blotting, the following Abs were used: Syn-1, Syn211, and 2628. The Syn-1 Ab, which recognizes aa 91–99, detected all mutant proteins, whereas the Syn211 Ab, which recognizes aa 121–125, did not detect all mutant proteins. The 2628 antibody, the exact specificity of which is unknown, detected wild type and ΔPR1 aS but not ΔPR2 and ΔC aS (Fig. 6*b*). Not only wild type aS but also mutant aS migrated to ~30–40 kDa (Fig. 6*c*). After the *in vitro* ubiquitination assay, all recombinant proteins were subjected to Western blotting using the Syn-1 Ab. We found that wild type aS produced high molecular weight bands in the presence of UbcH5b. In contrast, high molecular weight bands appeared less noticeable in samples containing these mutants (Fig. 6*d*). These results provide evidence that the PR sequence is required for aS ubiquitination by Nedd4-1. To further substantiate and extend these observations, SH-SY5Y cells were exposed to 5 μM wild type aS or to mutant aS lacking the PR sequence for 24 h. Intriguingly, we found that the endolysosomal as well as the cytosolic targeting of all mutants was greatly inhibited compared with that of wild type aS, whereas the PR mutation substantially increased the amount of re-secreted aS in the culture media (Fig. 6*e*). These results suggest that mutant aS forms that show disturbance in Nedd4-mediated polyubiquitination cannot be sorted into endolysosomal compartments. Furthermore, at least the nine amino acids (PR sequence ^{120}PDNEAYEMP^{128}) in the C terminus of aS may be required for endosomal targeting of aS by Nedd4-1.

Pro-120 and Pro-128 in the PR Sequence Are Essential for Nedd4-1-mediated Endosomal Targeting of aS—To further elucidate which proline residue(s) within the PR sequence are essential for the Nedd4-1-mediated aS ubiquitination, we generated recombinant aS in which proline 120 or proline 128 was replaced with alanine (P120A and P128A, respectively, in Fig. 7, *a* and *b*). Because HECT-type ubiquitin ligase sometimes attaches to phosphorylated serine/threonine residues (23), serine 129 (Ser-129), which is a major phosphorylation site in aS, was also substituted with alanine (S129A, in Fig. 7, *a* and *b*). After size exclusion filtration using a 100-kDa Amicon filter, all mutant aS and wild type aS migrated to ~40 kDa on BN-PAGE (Fig. 7*c*). *In vitro* ubiquitination assays using the UbcH5b E2 enzyme revealed that P120A and P128A aS mutants were less prone to being polyubiquitinated by Nedd4-1 compared with wild type aS, whereas the ubiquitination of S129A aS by Nedd4-1 was comparable with that of wild type-aS (Fig. 7*d*), suggesting that Pro-120 and Pro-128 are key residues for the Nedd4-1-mediated ubiquitination of aS. Intriguingly, we found that the level of intracellular aS was slightly decreased in P120A mutant aS, whereas P120A substitution substantially increased the amount of re-secreted aS in the culture media (Fig. 7*e*). Furthermore, subcellular fractionation analysis showed that the cytosolic and endosomal targeting of P120A and P128A mutants was disturbed compared with wild type and S129A aS. Cumulatively, these findings confirm the functional importance of the Pro-120 and Pro-128 residues for Nedd4-1-mediated endosomal targeting of aS.

DISCUSSION

One of the most exciting themes emerging from recent neurodegenerative research is the transcellular spread of pathogenic protein aggregates in affected brain lesions. To understand how aggregated proteins, such as aS, travel from cell to cell, the underlying mechanism responsible for the uptake and secretion of aggregate-prone proteins must be elucidated. The internalization of aS by cells is thought to be initiated by aS attachment to the outer leaflet of the plasma membrane via its amphipathic N-terminal domain (24, 25), which induces membrane curvature, tubulation, and breaking (26). Prior evidence has suggested that endocytic processes play a role in aS internalization in both neuronal and glial cells (3, 4, 27); however, aS internalization was not found to be completely blocked by the disruption of the endocytic machinery. These findings indicate that mechanisms other than endocytosis may contribute to aS internalization (3, 4, 27). Indeed, there is evidence showing that fibrillar and nonfibrillar oligomeric aS species are incorporated via the endocytic machinery and that monomeric aS directly passes through the plasma membrane (4). Unfortunately, how aS crosses the plasma membrane remains to be determined.

FIGURE 6. **C-terminal residues of aS are required for aS endosomal targeting mediated by Nedd4-1.** *a*, aS contains a relatively PR sequence at its C terminus (^{120}PDNEAYEMPSEEGYQDYEPEA^{140}). Three deletion mutants of aS, designated ΔPR1(1–119 and 129–140), ΔPR2(1–119 and 134–140), and ΔC(1–119), were generated to determine the functional importance of the PR motif in Nedd4-1-mediated ubiquitination. *b*, characterization of the aS deletion mutants by SDS-PAGE. Syn-1 antibody, which recognizes amino acids (*aa*) 91–99, detected all mutant proteins, whereas Syn211 antibody, which recognizes aa 121–125, did not detect all mutant proteins. The 2628 antibody, the exact specificity of which is unknown, detected wild type and ΔPR1 aS, but not ΔPR2 and ΔC aS. *c*, characterization of the aS deletion mutants by BN-PAGE. Both wild type aS and mutant aS migrated to ~30–40 kDa. *d*, *in vitro* ubiquitination assays using UbcH5b reveal that all of the PR mutants had a reduced ability to form Nedd4-1-mediated polyubiquitinated aS (*aS-Ub$_n$*). The densitometric values of aS-Ub$_n$ smear on long exposure image were normalized by the values of mono-aS on short exposure images ($p < 0.01$; each mutant is compared with wild type by Dunnett's multiple comparisons test). *e*, SH-SY5Y cells were exposed to 5 μM wild type and mutant aS lacking the PR sequence for 24 h and subjected to Western blot analysis. Note that the endolysosomal as well as the cytosolic targeting of all of the PR mutants was greatly inhibited compared with that of wild type aS, whereas the PR mutation substantially increased the amount of re-secreted aS in the medium (*asterisk*, $p < 0.01$; each mutant is compared with wild type by Dunnett's multiple comparisons test). The *right panel* shows the amount of monomeric aS normalized by each fraction marker. *IB*, immunoblot.

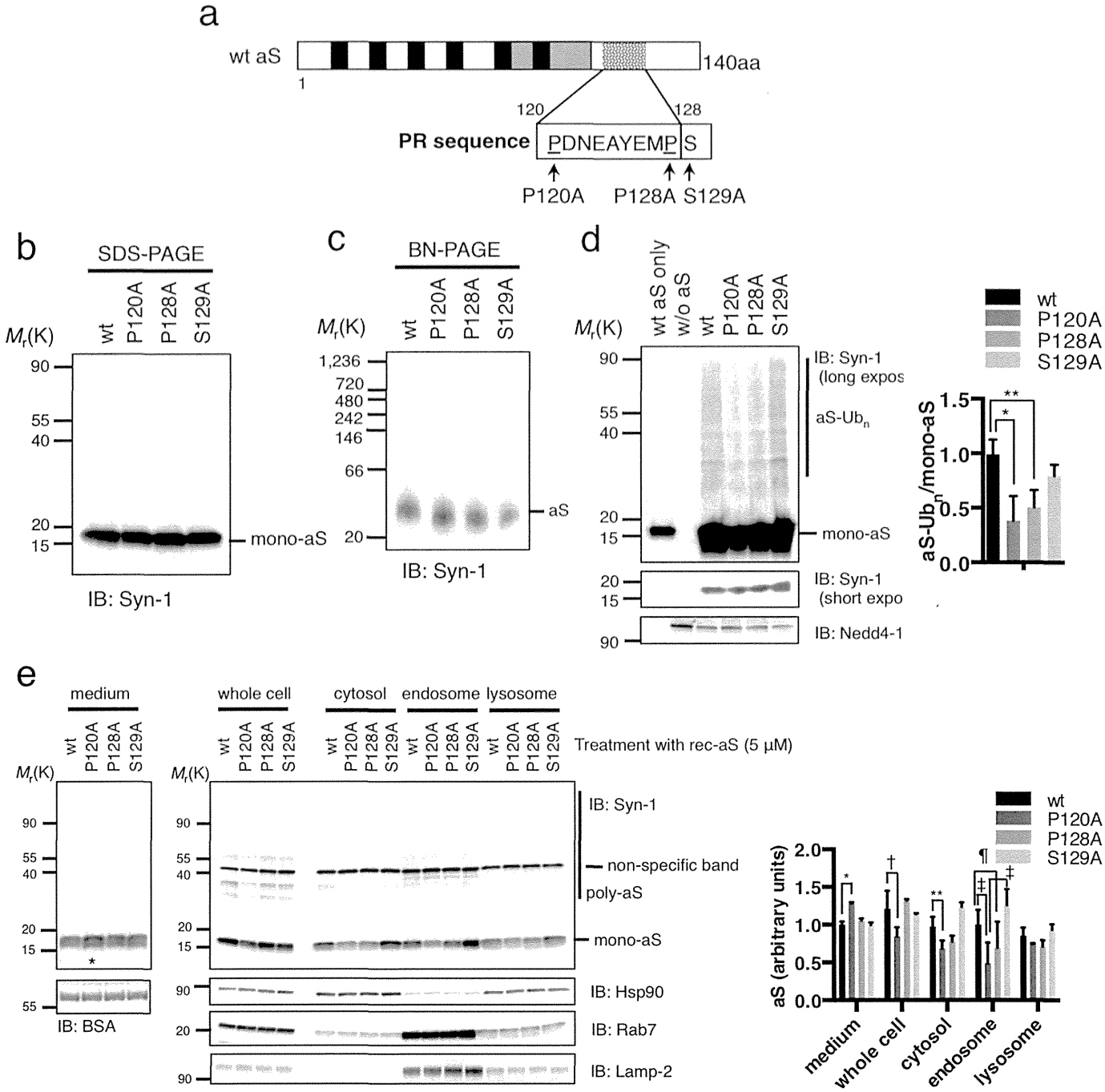

FIGURE 7. **Pro-120 might be a core frame of the aS PR sequence for Nedd4-1-mediated aS endosomal targeting.** *a,* schematic presentation of PR sequence (^{120}PDNEAYEMP^{128}) in human aS. The PR sequence contains two proline residues (Pro-120 and Pro-128), and Ser-129 flanks the PR sequence. *b,* characterization of the aS proline-substituted mutants by SDS-PAGE. All mutants appear as monomeric aS (15–20 kDa) under denaturing conditions. *c,* mutants and wild type aS (after 100-kDa size exclusion) showed LMW aS by BN-PAGE. *d, in vitro* ubiquitination assays using UbcH5b reveal that P120A and P128A aS mutants were less prone to polyubiquitination (*aS-Ub$_n$*) by Nedd4-1 compared with wild type aS, whereas the ubiquitination of S129A aS by Nedd4-1 was comparable with that of wild type-aS. The values for the amount of aS-Ub$_n$ from long exposure are divided by the values of mono-aS from short exposure (*asterisk*, $p < 0.01$; *double asterisk*, $p < 0.05$ by Dunnett's multiple comparisons test). *e,* SH-SY5Y cells were exposed to 5 μM wild type-aS or mutant, proline-substituted aS for 24 h and subjected to Western blot analysis. The levels of intracellular and cytosolic aS were slightly decreased in the P120A mutant aS (*dagger*, $p < 0.001$; *double asterisk*, $p < 0.05$), although this mutant substantially increased the amount of re-secreted aS in the culture media (*asterisk*, $p < 0.05$). Note that the cytosolic and endosomal targeting of P120A and P128A mutants was disturbed compared with wild type and S129A aS (*double dagger*, $p < 0.01$; *pilcrow*, $p < 0.05$ by Dunnett's multiple comparisons test). The *right panel* shows the amount of monomeric aS normalized by each fraction marker. *IB,* immunoblot.

Several possibilities have been postulated, including direct penetration (25), the formation of annular pore-like structures (28), and macropinocytosis (5, 29). Although this notion is provocative, it is supported by analogous studies in other neurodegenerative diseases, such as polyglutamine disease, in which polyQ aggregates can rapidly enter the cytosolic compartment of mammalian cells and nucleate the aggregation of soluble proteins with these polyQ tracts (30). Regardless of the mecha-

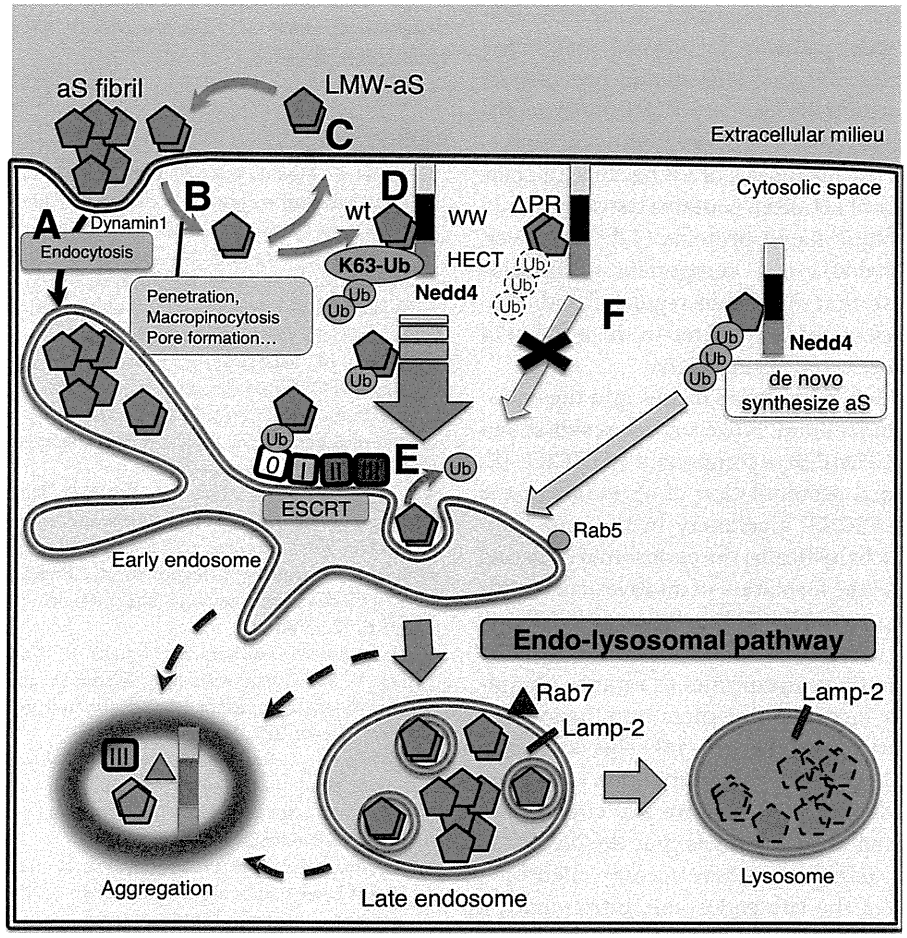

FIGURE 8. **Nedd4-1 determines the fate of internalized aS in neuronal cells.** Some extracellular aS is incorporated into neuronal cells by a dynamin-dependent mechanism and is transported into early endosomes (*A*). In contrast, a substantial amount of aS directly enters the cytosolic space, presumably via penetration of the plasma membrane (*B*). After crossing the plasma membrane, some of the internalized aS will exit the cells (*C*) and some will remain in the cytosol for minutes. Plasma membrane-resident Nedd4-1 binds to the C terminus of internalized aS through the WW domain and attaches a Lys-63-linked polyubiquitin chain to aS, thereby facilitating endosomal targeting (*D*). Most likely, the ESCRT complex recognizes the Lys-63-ubiquitinated aS and transports the aS into the late endosome through invagination of the endosomal membrane (*E*), which may promote aS degradation in lysosomes. The aS mutant that lacked the PR motif failed to sort into the late endosomes, most likely because it cannot be recognized by Nedd4-1 (*F*).

nisms involved in aS internalization, some extrinsic aS species can likely enter neuronal and/or glial cells directly, where they gain access to the cytosolic compartment and are subjected to further processing, modification, and transport.

In this study, we found that Nedd4-linked Lys-63 ubiquitination specified the fate of extrinsic and *de novo* synthesized aS by facilitating aS targeting to endosomal compartments. It appears that immediately after passing through the plasma membrane, the majority of the internalized aS is located just beneath the plasma membrane. Because Nedd4 localizes to the cytosolic space by associating with the inner plasma membrane leaflet via its C2 domain, Nedd4-1 likely preferentially catalyzes juxtamembrane aS localization. This notion is supported by previous studies showing that Nedd4-1-mediated ubiquitination is closely linked to the turnover and trafficking of cell-surface receptors (31, 32). Although aS does not contain the canonical PP*X*Y motif known to interact with the WW domain of Nedd4-1, the WW domain can recognize several motifs other than PP*X*Y with varying affinities (33). For example, the WW domains of Nedd4 families recognize PPLP, PR motifs, and phospho-(Ser/Thr) residues, as well as PP*X*Y (23). Our observation using deletion mutants provides evidence that the PR sequences in the C terminus of aS, particularly residues Pro-120 and Pro-128, are important for proper recognition by Nedd4-1. It is uncertain why Nedd4 silencing did not show a similar effect on the cytosolic aS accumulation as the ΔPR and P120A mutations. However, this could be attributed to the insufficient silencing efficacy of Nedd4 in cultured cells. The fact that a major phosphorylation site, Ser-129, occurs in the region flanking the aS PR sequence (34, 35) raises the possibility that phosphorylation at Ser-129 might affect Nedd4-1-mediated ubiquitination. However, this effect is not likely, as we found no difference in aS ubiquitination regardless of the presence of Ser-129.

Nedd4-1 catalyzes both the mono-ubiquitination and Lys-63-linked polyubiquitination of target proteins (36). Lys-63-linked ubiquitination is implicated in various cellular activities, including protein trafficking, DNA repair, stress responses, and signal transduction (37). Although mono-ubiquitination appears to be involved in endocytic trafficking, additional Lys-63-linked polyubiquitination is known to accelerate this trafficking process (38). More specifically, Lys-63-linked polyubiq-

uitination serves as a signal for protein sorting into the ESCRT-driven multivesicular body pathway by inward membrane invagination of endosomes (39). Previous studies have shown that LB showed immunoreactivity against ESCRT components such as CHMP2B and VPS4 (2, 40, 41). These findings are interesting when considering the biogenesis of LB because the pale body, a possible precursor of LB, often contains lysosomes, vacuolar structures, and ubiquitinated proteins (42). Moreover, our observation that Nedd4-1 is a component of LB also strengthens the hypothesis that the Nedd4-regulated endo/lysosomal sorting machinery might be involved in the buildup of aS-positive aggregates in affected brain lesions.

The mechanism by which cytosolic aS moves into the endosomal vesicle is poorly understood; however, our result showing that the silencing of CHMP2B, a component of ESCRT-III, can disrupt the endosomal accumulation of aS indicates the functional relevance of ESCRT machinery in the endolysosomal targeting of aS. Mechanistically, the endosomal targeting of ubiquitinated cargo and the formation of multivesicular bodies are mediated by the upstream ESCRT complexes (ESCRT-0, -I, and -II) on the surface of the endosomal membrane. ESCRT-III then recruits de-ubiquitinating enzymes to remove ubiquitin from the cargo before incorporating them into the intraluminal vesicles of multivesicular bodies (43, 44). This could be a reason why we failed to detect strong ubiquitination in aS-positive inclusions surrounded by Rab7-positive late endosomes. Another important finding of this study is that the Nedd4-1-mediated endosomal targeting of aS was accompanied by a prominent enlargement of the late endosome. Intriguingly, a marked enlargement of endosomal vesicles has also been shown in the affected brain and in a cellular model of Alzheimer disease (45, 46). Why the overexpression of Nedd4-1 downregulated the lysosomal accumulation of aS in this study is uncertain. One possible explanation is that the excessive accumulation of aS might prevent early-to-late endosome transition. Indeed, previous studies have shown that aS itself is closely involved in vesicular trafficking events, such as Rab-mediated endoplasmic reticulum-Golgi transport and endosomal trafficking (47–49). An alternative possibility is that aS aggregates may decrease the lysosomal burden by inducing lysosomal rupture (50).

In summary, we found that Nedd4-1 markedly facilitated aS internalization, which was linked to Lys-63 linkage-specific polyubiquitination. Our results demonstrate how Lys-63-linked ubiquitination contributes to the endosomal targeting and the endosomal accumulation of aS and therefore may be involved in the propagation and formation/clearance of Lewy pathology in PD (Fig. 8). Although the concept of the cell-to-cell transmission of aberrant proteins has been recognized as a common phenomenon in many neurodegenerative diseases, the molecular mechanisms underlying the spread of protein misfolding likely differ depending on the biochemical nature of the protein aggregate, the level of cellular stress, and the cell type. Further studies are needed to gain insight into the cellular mechanisms of disease progression and to identify molecular targets for therapeutic intervention in PD and other neurodegenerative diseases.

Acknowledgment—We are grateful to Nanae Osanai for excellent technical assistance.

REFERENCES

1. Angot, E., Steiner, J. A., Hansen, C., Li, J. Y., and Brundin, P. (2010) Are synucleinopathies prion-like disorders? *Lancet Neurol.* **9,** 1128–1138
2. Hasegawa, T., Konno, M., Baba, T., Sugeno, N., Kikuchi, A., Kobayashi, M., Miura, E., Tanaka, N., Tamai, K., Furukawa, K., Arai, H., Mori, F., Wakabayashi, K., Aoki, M., Itoyama, Y., and Takeda, A. (2011) The AAA-ATPase VPS4 regulates extracellular secretion and lysosomal targeting of α-synuclein. *PLoS One* **6,** e29460
3. Konno, M., Hasegawa, T., Baba, T., Miura, E., Sugeno, N., Kikuchi, A., Fiesel, F. C., Sasaki, T., Aoki, M., Itoyama, Y., and Takeda, A. (2012) Suppression of dynamin GTPase decreases α-synuclein uptake by neuronal and oligodendroglial cells: a potent therapeutic target for synucleinopathy. *Mol. Neurodegener.* **7,** 38
4. Lee, H. J., Suk, J. E., Bae, E. J., Lee, J. H., Paik, S. R., and Lee, S. J. (2008) Assembly-dependent endocytosis and clearance of extracellular α-synuclein. *Int. J. Biochem. Cell Biol.* **40,** 1835–1849
5. Lee, S. J., Desplats, P., Sigurdson, C., Tsigelny, I., and Masliah, E. (2010) Cell-to-cell transmission of non-prion protein aggregates. *Nat. Rev. Neurol.* **6,** 702–706
6. Hasegawa, M., Fujiwara, H., Nonaka, T., Wakabayashi, K., Takahashi, H., Lee, V. M., Trojanowski, J. Q., Mann, D., and Iwatsubo, T. (2002) Phosphorylated α-synuclein is ubiquitinated in α-synucleinopathy lesions. *J. Biol. Chem.* **277,** 49071–49076
7. Tofaris, G. K., Razzaq, A., Ghetti, B., Lilley, K. S., and Spillantini, M. G. (2003) Ubiquitination of α-synuclein in Lewy bodies is a pathological event not associated with impairment of proteasome function. *J. Biol. Chem.* **278,** 44405–44411
8. Kuzuhara, S., Mori, H., Izumiyama, N., Yoshimura, M., and Ihara, Y. (1988) Lewy bodies are ubiquitinated. A light and electron microscopic immunocytochemical study. *Acta Neuropathol.* **75,** 345–353
9. Tofaris, G. K., Kim, H. T., Hourez, R., Jung, J. W., Kim, K. P., and Goldberg, A. L. (2011) Ubiquitin ligase Nedd4 promotes α-synuclein degradation by the endosomal-lysosomal pathway. *Proc. Natl. Acad. Sci. U.S.A.* **108,** 17004–17009
10. Davies, S. E., Hallett, P. J., Moens, T., Smith, G., Mangano, E., Kim, H. T., Goldberg, A. L., Liu, J. L., Isacson, O., and Tofaris, G. K. (2014) Enhanced ubiquitin-dependent degradation by Nedd4 protects against α-synuclein accumulation and toxicity in animal models of Parkinson's disease. *Neurobiol. Dis.* **64,** 79–87
11. Staub, O., Dho, S., Henry, P., Correa, J., Ishikawa, T., McGlade, J., and Rotin, D. (1996) WW domains of Nedd4 bind to the proline-rich PY motifs in the epithelial Na^+ channel deleted in Liddle's syndrome. *EMBO J.* **15,** 2371–2380
12. Kanelis, V., Bruce, M. C., Skrynnikov, N. R., Rotin, D., and Forman-Kay, J. D. (2006) Structural determinants for high-affinity binding in a Nedd4 WW3* domain-Comm PY motif complex. *Structure* **14,** 543–553
13. Wang, J., Peng, Q., Lin, Q., Childress, C., Carey, D., and Yang, W. (2010) Calcium activates Nedd4 E3 ubiquitin ligases by releasing the C2 domain-mediated auto-inhibition. *J. Biol. Chem.* **285,** 12279–12288
14. Dunn, R., and Hicke, L. (2001) Multiple roles for Rsp5p-dependent ubiquitination at the internalization step of endocytosis. *J. Biol. Chem.* **276,** 25974–25981
15. Hara, S., Arawaka, S., Sato, H., Machiya, Y., Cui, C., Sasaki, A., Koyama, S., and Kato, T. (2013) Serine 129 phosphorylation of membrane-associated α-synuclein modulates dopamine transporter function in a G protein-coupled receptor kinase-dependent manner. *Mol. Biol. Cell* **24,** 1649–1660
16. Schröter, C. J., Braun, M., Englert, J., Beck, H., Schmid, H., and Kalbacher, H. (1999) A rapid method to separate endosomes from lysosomal contents using differential centrifugation and hypotonic lysis of lysosomes. *J. Immunol. Methods* **227,** 161–168
17. Rott, R., Szargel, R., Haskin, J., Shani, V., Shainskaya, A., Manov, I., Liani, E., Avraham, E., and Engelender, S. (2008) Monoubiquitylation of α-sy-

nuclein by seven in absentia homolog (SIAH) promotes its aggregation in dopaminergic cells. *J. Biol. Chem.* **283,** 3316–3328
18. Nagano, Y., Yamashita, H., Takahashi, T., Kishida, S., Nakamura, T., Iseki, E., Hattori, N., Mizuno, Y., Kikuchi, A., and Matsumoto, M. (2003) Siah-1 facilitates ubiquitination and degradation of synphilin-1. *J. Biol. Chem.* **278,** 51504–51514
19. Shimura, H., Schlossmacher, M. G., Hattori, N., Frosch, M. P., Trockenbacher, A., Schneider, R., Mizuno, Y., Kosik, K. S., and Selkoe, D. J. (2001) Ubiquitination of a new form of α-synuclein by parkin from human brain: implications for Parkinson's disease. *Science* **293,** 263–269
20. Tetzlaff, J. E., Putcha, P., Outeiro, T. F., Ivanov, A., Berezovska, O., Hyman, B. T., and McLean, P. J. (2008) CHIP targets toxic α-Synuclein oligomers for degradation. *J. Biol. Chem.* **283,** 17962–17968
21. Anan, T., Nagata, Y., Koga, H., Honda, Y., Yabuki, N., Miyamoto, C., Kuwano, A., Matsuda, I., Endo, F., Saya, H., and Nakao, M. (1998) Human ubiquitin-protein ligase Nedd4: expression, subcellular localization and selective interaction with ubiquitin-conjugating enzymes. *Genes Cells* **3,** 751–763
22. Nikko, E., and André, B. (2007) Evidence for a direct role of the Doa4 deubiquitinating enzyme in protein sorting into the MVB pathway. *Traffic* **8,** 566–581
23. Lu, P. J., Zhou, X. Z., Shen, M., and Lu, K. P. (1999) Function of WW domains as phosphoserine- or phosphothreonine-binding modules. *Science* **283,** 1325–1328
24. Georgieva, E. R., Ramlall, T. F., Borbat, P. P., Freed, J. H., and Eliezer, D. (2010) The lipid-binding domain of wild type and mutant α-synuclein: compactness and interconversion between the broken and extended helix forms. *J. Biol. Chem.* **285,** 28261–28274
25. Ahn, K. J., Paik, S. R., Chung, K. C., and Kim, J. (2006) Amino acid sequence motifs and mechanistic features of the membrane translocation of α-synuclein. *J. Neurochem.* **97,** 265–279
26. Varkey, J., Isas, J. M., Mizuno, N., Jensen, M. B., Bhatia, V. K., Jao, C. C., Petrlova, J., Voss, J. C., Stamou, D. G., Steven, A. C., and Langen, R. (2010) Membrane curvature induction and tubulation are common features of synucleins and apolipoproteins. *J. Biol. Chem.* **285,** 32486–32493
27. Desplats, P., Lee, H. J., Bae, E. J., Patrick, C., Rockenstein, E., Crews, L., Spencer, B., Masliah, E., and Lee, S. J. (2009) Inclusion formation and neuronal cell death through neuron-to-neuron transmission of α-synuclein. *Proc. Natl. Acad. Sci. U.S.A.* **106,** 13010–13015
28. Tsigelny, I. F., Sharikov, Y., Wrasidlo, W., Gonzalez, T., Desplats, P. A., Crews, L., Spencer, B., and Masliah, E. (2012) Role of α-synuclein penetration into the membrane in the mechanisms of oligomer pore formation. *FEBS J.* **279,** 1000–1013
29. Lashuel, H. A., Overk, C. R., Oueslati, A., and Masliah, E. (2013) The many faces of α-synuclein: from structure and toxicity to therapeutic target. *Nat. Rev. Neurosci.* **14,** 38–48
30. Ren, P. H., Lauckner, J. E., Kachirskaia, I., Heuser, J. E., Melki, R., and Kopito, R. R. (2009) Cytoplasmic penetration and persistent infection of mammalian cells by polyglutamine aggregates. *Nat. Cell Biol.* **11,** 219–225
31. Lin, A., Hou, Q., Jarzylo, L., Amato, S., Gilbert, J., Shang, F., and Man, H. Y. (2011) Nedd4-mediated AMPA receptor ubiquitination regulates receptor turnover and trafficking. *J. Neurochem.* **119,** 27–39
32. Nabhan, J. F., Pan, H., and Lu, Q. (2010) Arrestin domain-containing protein 3 recruits the NEDD4 E3 ligase to mediate ubiquitination of the β2-adrenergic receptor. *EMBO Rep.* **11,** 605–611
33. Ingham, R. J., Gish, G., and Pawson, T. (2004) The Nedd4 family of E3 ubiquitin ligases: functional diversity within a common modular architecture. *Oncogene* **23,** 1972–1984
34. Fujiwara, H., Hasegawa, M., Dohmae, N., Kawashima, A., Masliah, E., Goldberg, M. S., Shen, J., Takio, K., and Iwatsubo, T. (2002) α-Synuclein is phosphorylated in synucleinopathy lesions. *Nat. Cell Biol.* **4,** 160–164
35. Sugeno, N., Takeda, A., Hasegawa, T., Kobayashi, M., Kikuchi, A., Mori, F., Wakabayashi, K., and Itoyama, Y. (2008) Serine 129 phosphorylation of α-synuclein induces unfolded protein response-mediated cell death. *J. Biol. Chem.* **283,** 23179–23188
36. Rotin, D., and Kumar, S. (2009) Physiological functions of the HECT family of ubiquitin ligases. *Nat. Rev. Mol. Cell Biol.* **10,** 398–409
37. Lauwers, E., Jacob, C., and André, B. (2009) Lys-63-linked ubiquitin chains as a specific signal for protein sorting into the multivesicular body pathway. *J. Cell Biol.* **185,** 493–502
38. Galan, J. M., and Haguenauer-Tsapis, R. (1997) Ubiquitin lys63 is involved in ubiquitination of a yeast plasma membrane protein. *EMBO J.* **16,** 5847–5854
39. Lauwers, E., Erpapazoglou, Z., Haguenauer-Tsapis, R., and André, B. (2010) The ubiquitin code of yeast permease trafficking. *Trends Cell Biol.* **20,** 196–204
40. Tanikawa, S., Mori, F., Tanji, K., Kakita, A., Takahashi, H., and Wakabayashi, K. (2012) Endosomal sorting related protein CHMP2B is localized in Lewy bodies and glial cytoplasmic inclusions in α-synucleinopathy. *Neurosci. Lett.* **527,** 16–21
41. Kurashige, T., Takahashi, T., Yamazaki, Y., Hiji, M., Izumi, Y., Yamawaki, T., and Matsumoto, M. (2013) Localization of CHMP2B-immunoreactivity in the brainstem of Lewy body disease. *Neuropathology* **33,** 237–245
42. Hayashida, K., Oyanagi, S., Mizutani, Y., and Yokochi, M. (1993) An early cytoplasmic change before Lewy body maturation: an ultrastructural study of the substantia nigra from an autopsy case of juvenile parkinsonism. *Acta Neuropathol.* **85,** 445–448
43. Williams, R. L., and Urbé, S. (2007) The emerging shape of the ESCRT machinery. *Nat. Rev. Mol. Cell Biol.* **8,** 355–368
44. Agromayor, M., and Martin-Serrano, J. (2006) Interaction of AMSH with ESCRT-III and deubiquitination of endosomal cargo. *J. Biol. Chem.* **281,** 23083–23091
45. Cataldo, A. M., Peterhoff, C. M., Troncoso, J. C., Gomez-Isla, T., Hyman, B. T., and Nixon, R. A. (2000) Endocytic pathway abnormalities precede amyloid β deposition in sporadic Alzheimer's disease and Down syndrome: differential effects of APOE genotype and presenilin mutations. *Am. J. Pathol.* **157,** 277–286
46. Nixon, R. A. (2004) Niemann-Pick type C disease and Alzheimer's disease: the APP-endosome connection fattens up. *Am. J. Pathol.* **164,** 757–761
47. Gitler, A. D., Bevis, B. J., Shorter, J., Strathearn, K. E., Hamamichi, S., Su, L. J., Caldwell, K. A., Caldwell, G. A., Rochet, J. C., McCaffery, J. M., Barlowe, C., and Lindquist, S. (2008) The Parkinson's disease protein α-synuclein disrupts cellular Rab homeostasis. *Proc. Natl. Acad. Sci. U.S.A.* **105,** 145–150
48. Soper, J. H., Kehm, V., Burd, C. G., Bankaitis, V. A., and Lee, V. M. (2011) Aggregation of α-synuclein in *S. cerevisiae* is associated with defects in endosomal trafficking and phospholipid biosynthesis. *J. Mol. Neurosci.* **43,** 391–405
49. Tardiff, D. F., Jui, N. T., Khurana, V., Tambe, M. A., Thompson, M. L., Chung, C. Y., Kamadurai, H. B., Kim, H. T., Lancaster, A. K., Caldwell, K. A., Caldwell, G. A., Rochet, J. C., Buchwald, S. L., and Lindquist, S. (2013) Yeast reveal a "Druggable" Rsp5/Nedd4 network that ameliorates α-synuclein toxicity in neurons. *Science* **342,** 979–983
50. Freeman, D., Cedillos, R., Choyke, S., Lukic, Z., McGuire, K., Marvin, S., Burrage, A. M., Sudholt, S., Rana, A., O'Connor, C., Wiethoff, C. M., and Campbell, E. M. (2013) α-Synuclein induces lysosomal rupture and cathepsin-dependent reactive oxygen species following endocytosis. *PLoS One* **8,** e62143

Increased α-synuclein levels in the cerebrospinal fluid of patients with Creutzfeldt–Jakob disease

Takashi Kasai, Takahiko Tokuda, Ryotaro Ishii, Noriko Ishigami, Yoshio Tsuboi, Masanori Nakagawa, Toshiki Mizuno & Omar M. A. El-Agnaf

Journal of Neurology
Official Journal of the European Neurological Society

ISSN 0340-5354

J Neurol
DOI 10.1007/s00415-014-7334-7

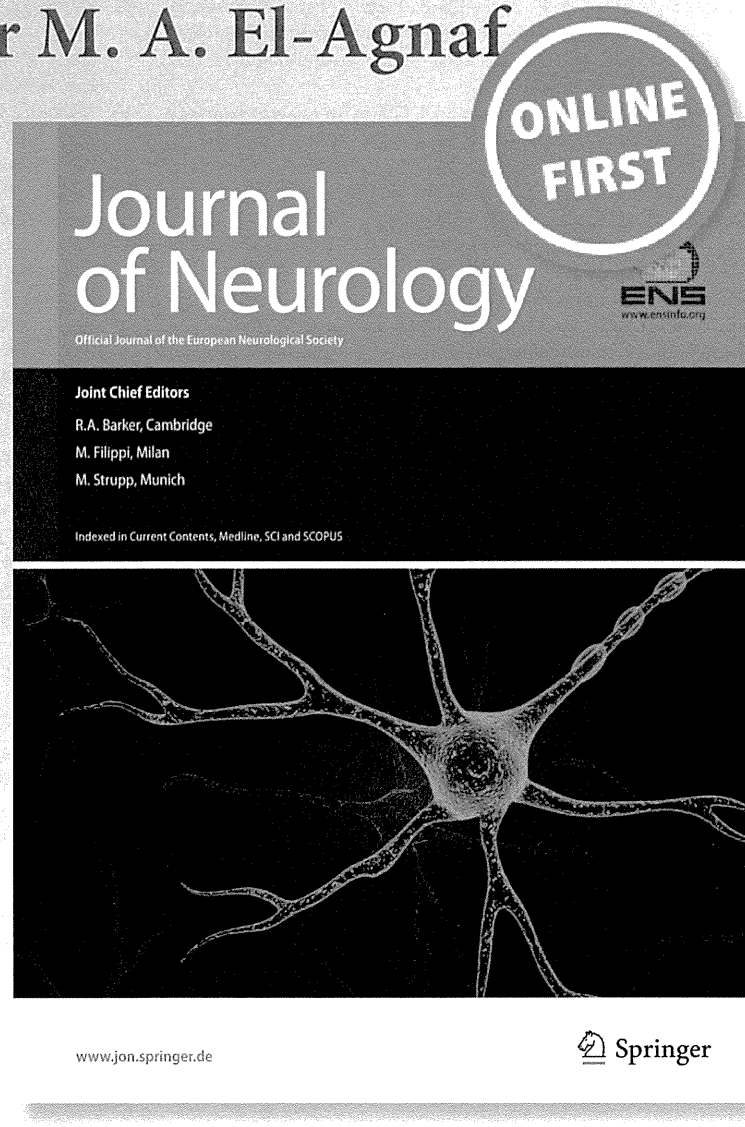

Springer

J Neurol
DOI 10.1007/s00415-014-7334-7

ORIGINAL COMMUNICATION

Increased α-synuclein levels in the cerebrospinal fluid of patients with Creutzfeldt–Jakob disease

Takashi Kasai · Takahiko Tokuda · Ryotaro Ishii · Noriko Ishigami · Yoshio Tsuboi · Masanori Nakagawa · Toshiki Mizuno · Omar M. A. El-Agnaf

Received: 13 January 2014 / Revised: 25 March 2014 / Accepted: 26 March 2014

Abstract Recent studies have shown that cerebrospinal fluid (CSF) levels of α-synuclein (α-syn) are highly elevated in patients with Creutzfeldt–Jakob disease (CJD) compared to controls. However, the diagnostic value of CSF α-syn in CJD has not been established. To confirm whether CSF α-syn is increased in CJD and is a useful marker for this disease, two independent enzyme-linked immunoabsorbent assays (ELISAs) specific for α-syn were used: ELISA 211-FL140, which is specific for full-length α-syn, and ELISA N19-FL140, which is specific for the full-length and associated C-terminal truncated forms of α-syn. CSF samples from 24 patients with CJD and 24 controls were assessed in this study. We found that samples from the CJD patients showed significantly higher levels of CSF α-syn compared to controls in both ELISA (211-FL140 or N19-FL140) tests ($P = 0.0467$ and $P = 0.0010$, respectively). However, there was a considerable overlap in the concentration ranges of the two groups of subjects. We also measured the levels of total tau (t-tau) protein in these samples and found that CSF t-tau levels were 5–10-times higher in the CJD group ($P < 0.0001$) compared with the controls. When the CSF t-tau and α-syn levels were combined, the area under the ROC curve (AUC) was slightly increased in clinically diagnosed CJD cases (AUC of 0.964) relative to an AUC of 0.943 for increased CSF t-tau alone. The combined use of CSF α-syn and t-tau levels may be a useful biomarker for the diagnosis of CJD.

Keywords Creutzfeldt–Jakob disease · Cerebrospinal fluid · α-Synuclein · Tau · Biomarker · ELISA

Introduction

Creutzfeldt–Jakob disease (CJD) is a rare neurodegenerative disease that mainly affects elderly people. The diagnosis of CJD can only be confirmed by brain biopsy; however, certain biochemical markers in cerebrospinal fluid (CSF) have been reported to be useful in the differential diagnosis of CJD from other dementia-spectrum illnesses. Several reports have demonstrated that total tau protein (t-tau) in the CSF is one of the most sensitive biomarkers in the early diagnosis of CJD [1, 2]. Tau is a microtubule-associated protein that contributes to axonal structure [3]. Therefore, axonal degeneration and the leakage of axonal proteins in the brains of CJD patients are the most likely causes of an increase in CSF levels of t-tau. However, the primary neuropathological feature in prion diseases is the loss of synapses rather than axonal degeneration [4–6], and proteins leaking from synaptic structures probably have a greater early diagnostic value than t-tau or other axonal proteins in CJD. Therefore, we investigated

Electronic supplementary material The online version of this article (doi:10.1007/s00415-014-7334-7) contains supplementary material, which is available to authorized users.

T. Kasai (✉) · T. Tokuda · R. Ishii · N. Ishigami · M. Nakagawa · T. Mizuno
Department of Neurology, Research Institute for Geriatrics, Kyoto Prefectural University of Medicine, Kyoto 602-0841, Japan
e-mail: kasaita@koto.kpu-m.ac.jp

Y. Tsuboi
Department of Neurology, Fukuoka University School of Medicine, Fukuoka 814-0180, Japan

O. M. A. El-Agnaf
Department of Biochemistry, Faculty of Medicine and Health Sciences, United Arab Emirates University, Al Ain, United Arab Emirates

Published online: 16 April 2014

the levels of the synaptic protein α-synuclein (α-syn) in CSF from patients with CJD and healthy matched controls.

α-Syn is a protein involved in the pathogenesis of Parkinson's disease (PD) and other synucleinopathies. Recently, our group and others have developed protocols for sandwich-type enzyme-linked immunoabsorbent assays (ELISAs) specific for α-syn and have reported decreased CSF levels of α-syn in patients with PD compared to controls [7–10]. Interestingly, it has been reported that CSF levels of α-syn were highly elevated in eight CJD patients compared with controls [9]. The strong increase in the CSF levels of α-syn in CJD patients was interpreted as biochemical evidence of rapid synaptic degeneration and leakage of α-syn, which is known to be a major component of presynaptic proteins [11], in CJD. Although it has been implied that CSF α-syn could be a diagnostic marker for CJD, relatively few patients have been studied, and thus study size has been insufficient for evaluating the diagnostic value. To verify these previous findings and to evaluate the diagnostic utility of CSF α-syn for CJD, we investigated the levels of α-syn in CSF from 24 patients with CJD and 24 control subjects.

Methods and materials

Patients

CSF samples were collected from 24 patients with CJD (age 41–82, mean ± SD = 62.9 ± 10.0) and 24 gender- and age-matched control subjects (age 17–88, mean ± SD = 60.0 ± 18.3). The CJD group included two patients with familial CJD (V180I), three patients with probable iatrogenic CJD (iCJD) and 19 patients with probable sporadic CJD (sCJD). Probable sCJD and iCJD patients fulfilled the WHO diagnostic criteria for CJD [12]. The control group included neurologically normal individuals ($n = 8$) as well as subjects with peripheral neuropathy ($n = 8$), cranial neuropathy ($n = 3$), epilepsy ($n = 2$), motor neuron disease ($n = 1$), spastic paraplegia ($n = 1$), and spinal myoclonus ($n = 1$). Informed consent was obtained from the patient when possible or from the nearest relative when not possible, which was approved by the University Ethics Committee (Kyoto Prefectural University of Medicine, Kyoto, and the Fukuoka University School of Medicine, Fukuoka, Japan). The study procedures were designed and performed in accordance with the Declaration of Helsinki. Fresh CSF samples collected from living CJD patients and control cases were cleared by centrifugation at 3,000×g for 10 min at 4 °C and then stored at −80 °C until used for this study. We excluded samples with apparent blood contamination from this study following visual inspection of centrifuged CSF. Samples with pink-red discoloration indicative of hemoglobinemia were excluded.

Antibodies

The anti-human α-syn monoclonal antibody 211 (MAb211) recognizes the C-terminal portion of α-syn (residues 121–125). The anti-human α-/β-synuclein goat polyclonal antibody N19 recognizes the N-terminal portion of α-syn (residues 5–19). The anti-human α-/β-/γ-synuclein rabbit polyclonal antibody FL-140 was raised against the recombinant full-length α-syn (Fig. 1a). All antibodies were purchased from Santa Cruz Biotechnology, CA, USA.

Measurement of α-syn

CSF α-syn levels were measured using a previously reported sandwich ELISA system that was modified to achieve an improved sensitivity as low as 0.01 pg/ml [7]. Briefly, each ELISA plate (384-well ELISA plate, Nunc Maxisorb™, NUNC A/S, Roskilde, Denmark) was coated with 1 μg/ml of either MAb211 or N19 antibodies (50 μl/well) as a capture antibody in 200 mM $NaHCO_3$, pH 9.6, at 4 °C for overnight. The plate was then washed with phosphate buffered saline (PBS) containing 0.05 % Tween 20 (PBST) and subsequently incubated with 100 μl/well of a blocking buffer (PBST containing 2.5 % gelatin) for 2 h at 37 °C. After adding a cocktail of protease inhibitors (Calbiochem, CA, USA) to the CSF samples, 50 μl of these samples were added to each well and the plate was incubated at 37 °C for 3 h. After washing with PBST, 50 μl of anti-α-syn antibody FL-140 (0.2 mg/ml in the blocking buffer) was added as a reporter antibody, and the plate was incubated at 37 °C for 2 h. After washing with PBST, the wells were incubated with 50 μl/well of horseradish peroxidase (HRP)-labeled anti-rabbit immunoglobulins (DAKO, Glostrup, Denmark) and incubated for 1 h at 37°C. Bound HRP activity was assayed using an enhanced chemiluminescent substrate (SuperSignal Femto Maximum Sensitivity Substrate, Pierce Biotechnology, Rockford, IL, USA, 50 μl/well), and the chemiluminescence signal was measured at 395 nm with a microplate luminometer (SpectraMax L, Molecular Devices, Tokyo, Japan). The standard curve for the ELISA was prepared using 50 μl/well of recombinant human α-syn solution at different concentrations of the protein in PBS solution. All samples and standards were run in triplicate on the same day with the same lot of standards unless otherwise noted. The relative estimated concentrations of CSF α-syn were calculated using a standard curve. In the following descriptions, the use of MAb211 as the capture antibody and FL140 as the reporter antibody is referred to as "211-FL140 ELISA", and the use of N19 as the capture antibody and

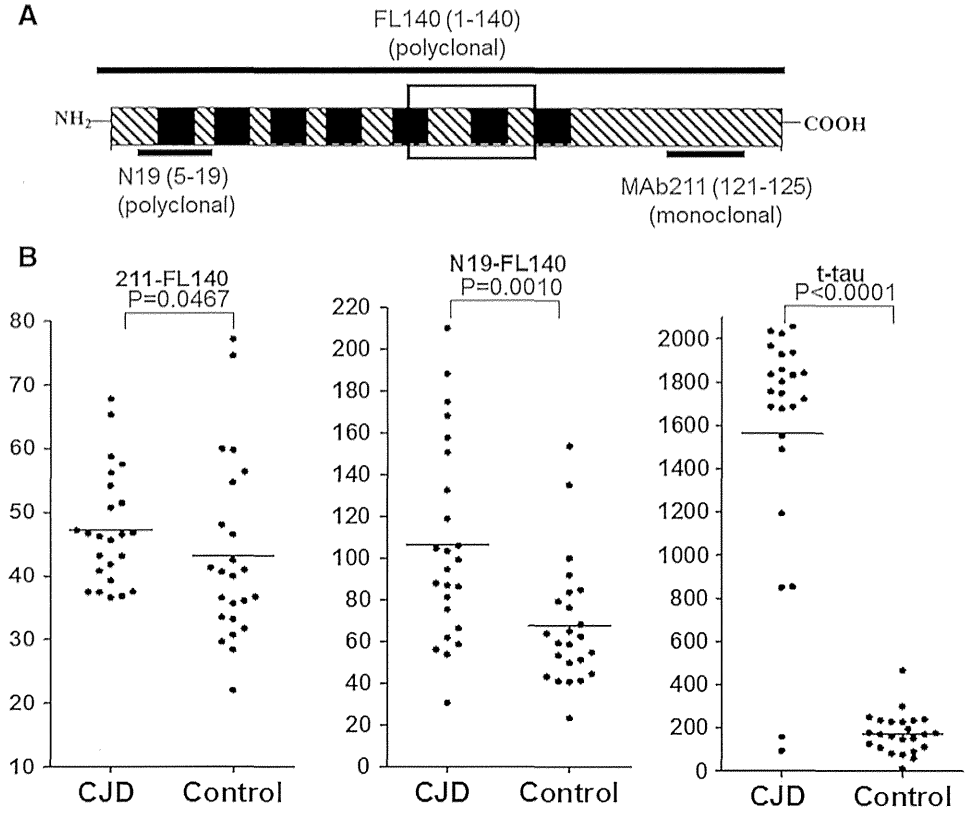

Fig. 1 **a** Recognition sequences for α-syn antibodies. Recognition sequences for α-syn antibodies used in the present study are shown as *black bars* in the schema of the primary structure of α-syn. *Black boxes* indicate imperfect lysine-rich motifs (KTKEGV), and the *white box* indicates the non-amyloid-β component (NAC) domain. **b** Scatter plots of the levels of CSF α-syn, measured using 211-FL140 ELISA and N19-FL140 ELISA, and the levels of t-tau. The CSF α-syn concentrations measured with two ELISA methods, 211-FL140 ELISA, N19-FL140 ELISA, and the t-tau levels measured using a commercial kit are shown. The concentrations of CSF α-syn in the CJD group were significantly higher than that in the age-matched control subjects for either ELISA ($P = 0.0467$ using 211-FL140 ELISA, and $P = 0.0010$ using N19-FL140 ELISA, Mann–Whitney U test). The levels of t-tau were highly elevated in the CJD group ($P < 0.0001$, Mann–Whitney U test)

FL140 as the reporter antibody is referred to as "N19-FL140 ELISA". The 211-FL140 ELISA is specific for the full-length human α-syn because of the selective affinity of MAb211 for α-syn. In contrast, N19 recognizes the N-terminal sequence of α-syn, which is shared by β-synuclein (β-syn) (Fig. 1a); therefore, N19-FL140 ELISA can detect both proteins. However, using mass spectroscopy, we have reported that neither β-syn nor γ-synuclein was detected in human CSF [9], and therefore, our N19-FL140 ELISA array only measures the α-syn present in CSF. It is noteworthy that this ELISA protocol can also detect the C-terminal truncated forms of α-syn present in CSF, which cannot be detected by the 211-FL140 ELISA protocol.

Measurement of t-tau

The levels of CSF t-tau were measured using the Fino Scholar hTau ELISA kit (Nipro, Osaka, Japan) according to the manufacturer's instructions.

Statistics

Image analysis was performed using Scion Image for Windows Version 4 (Scion Corporation Frederick, MA, USA). A comparison between the two independent groups was performed using the Mann–Whitney U test. The ROC curve and the AUC were calculated and compared between the two α-syn ELISA arrays. $P < 0.05$ was considered statically significant. Statistical analyses were performed using GraphPad Prism Version 4.0 (GraphPad Software, San Diego, CA, USA).

Results

As shown in Fig. 1b, the concentrations of CSF α-syn measured using the 211-FL140 ELISA were significantly higher in CJD patients than in controls (mean ± SD; 47.28 ± 8.98 in CJD vs. 42.33 ± 12.53 in controls,

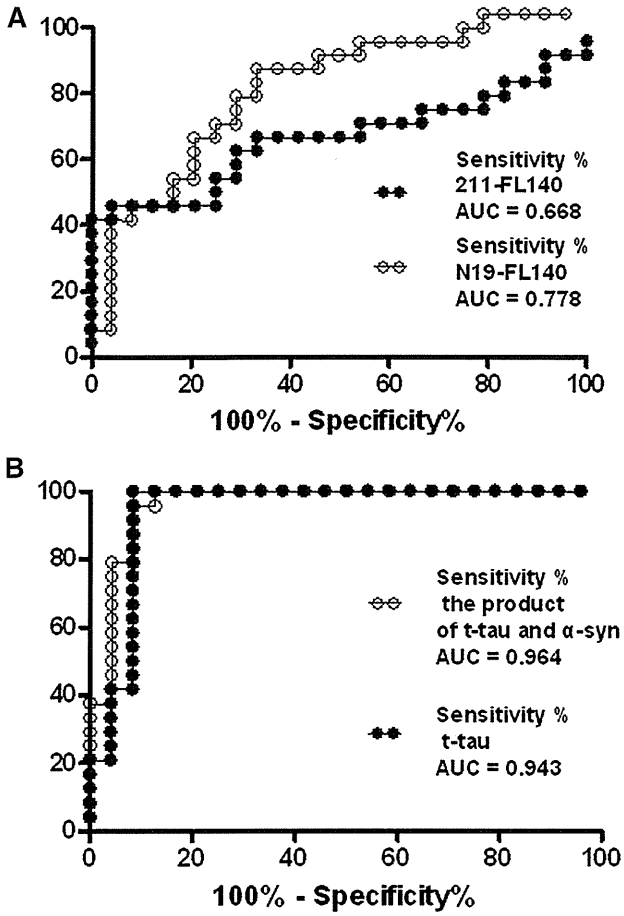

Fig. 2 **a** Receiver operating characteristic (ROC) curves for the levels of α-syn in CSF in the discrimination of patients with CJD from controls when using the 211-FL140 ELISA (*black circles*) and the N19-FL140 ELISA (*white circles*). AUC values are indicated. **b** ROC curves for the use of t-tau alone (*black circles*) and the use of combined t-tau and α-syn (*white circles*) in the discrimination of patients with CJD from controls. AUC values are indicated

$P = 0.0467$). However, there was a considerable overlap in the concentration ranges for the two groups. Receiver operating characteristic (ROC) curves used to discriminate patients with CJD from the control subjects were calculated based on ELISA data. The area under the ROC curve (AUC) for the 211-FL140 ELISA was poor (AUC = 0.668) (Fig. 2a). Using the N19-FL140 ELISA, significantly higher levels of CSF α-syn were detected in CJD patients than in controls (mean ± SD; 106.3 ± 47.23 in CJD vs. 66.38 ± 26.76 in controls, $P = 0.0010$). The AUC in the ROC curve used to discriminate CJD patients from controls improved in the N19-FL140 ELISA (AUC = 0.778) (Fig. 2a), although an overlap in the concentration ranges for the two groups was still observed, and the mean value of the signals in the CJD group was no more than twice that of the control group.

We also measured the levels of total tau (t-tau) in CJD and control samples. The mean value of t-tau in controls corresponded with previously reported levels (mean ± SD; 188 ± 103 pg/ml) [13].The CSF levels of t-Tau were highly elevated in the CJD group ($P < 0.0001$, Mann–Whitney U test) with mean values 5–10-times higher than in control patients (mean ± SD; 1,564.11 ± 548.16 pg/ml in CJD vs. 173.77 ± 93.57 pg/ml in controls). However, two CJD patients who had normal levels of CSF t-tau also had elevated levels of CSF α-syn, as measured with the N19-FL140 ELISA (87.8 and 105.8 ng/ml), that exceeded the threshold value of 77.7 ng/ml. The measured levels of CSF t-tau and α-syn in CJD patients are summarized in Table 1. When we calculated the values of t-tau and α-syn measured with the N19-FL140 ELISA, the AUC of the product (0.964) was slightly higher than that of t-tau alone (0.943) in the ROC analysis (Fig. 2b). The optimized threshold value of the product was 14,922 ng/ml, where the sensitivity and specificity of the test were 79.17 and 95.83 %, respectively.

Discussion

The CSF levels of α-syn measured with the 211-FL140 ELISA were significantly higher in CJD patients than in controls. Our data is in agreement with the results reported by Mollenhauer et al. [9]. In this earlier report, CSF α-syn levels in CJD were more than 40 times higher than in controls [9], whereas our results recorded a sizeable overlap between the concentration ranges for individual signals for CJD patients and controls. Such a discrepancy could be caused by the narrow binding specificity of MAb211, which only binds to the full-length α-syn [14]; thus, an alternative assay system (N19-FL140 ELISA) was developed in which full-length α-syn and its C-terminal truncated forms are detectable. Interestingly, the N19-FL140 assay showed better diagnostic performance than did the 211-FL140 assay. However, the large signal difference between the CJD patients and the control group reported by Mollenhauer and co-workers [9] was not reproduced in our current study. Such inconsistencies among different studies may be caused by methodological issues, including pre-analytical differences in the collection, handling, and storage of CSF samples as well as the use of antibodies that detect different species of α-syn. In fact, when we performed immunoprecipitation followed by western blotting as an alternative approach to roughly estimate the CSF α-syn levels detected with ELISA, we found that the density of the band for full-length α-syn in CJD patients was much higher than that in controls in IP-WB (Supplementary Figure). We currently have no clear